






Direct targeting of FOXP3 in Tregs with AZD8701, a novel antisense oligonucleotide to relieve immunosuppression in cancer

Alexey Revenko ¹, Larissa S Carnevalli ², Charles Sinclair,² Ben Johnson,¹ Alison Peter,² Molly Taylor,² Lisa Hettrick,¹ Melissa Chapman,³ Stephanie Klein,¹ Anisha Solanki,² Danielle Gattis,¹ Andrew Watt,¹ Adina M Hughes ², Lukasz Magiera,² Gozde Kar,² Lucy Ireland,² Deanna A Mele ⁴, Vasu Sah,⁴ Maneesh Singh,⁴ Josephine Walton,² Maelle Mairesse,⁴ Matthew King,² Mark Edbrooke,² Paul Lyne,⁴ Simon T Barry,² Stephen Fawell,⁴ Frederick W Goldberg ², A Robert MacLeod¹

To cite: Revenko A, Carnevalli LS, Sinclair C, *et al.* Direct targeting of FOXP3 in Tregs with AZD8701, a novel antisense oligonucleotide to relieve immunosuppression in cancer. *Journal for ImmunoTherapy of Cancer* 2022;**10**:e003892. doi:10.1136/jitc-2021-003892

► Additional supplemental material is published online only. To view, please visit the journal online (<http://dx.doi.org/10.1136/jitc-2021-003892>).

AR, LSC and CS contributed equally.

Accepted 21 February 2022



© Author(s) (or their employer(s)) 2022. Re-use permitted under CC BY-NC. No commercial re-use. See rights and permissions. Published by BMJ.

For numbered affiliations see end of article.

Correspondence to

Dr A Robert MacLeod;
rob.macleod@flamingotx.com

Dr Frederick W Goldberg;
frederick.goldberg@astrazeneca.com

ABSTRACT

Background The Regulatory T cell (Treg) lineage is defined by the transcription factor FOXP3, which controls immune-suppressive gene expression profiles. Tregs are often recruited in high frequencies to the tumor microenvironment where they can suppress antitumor immunity. We hypothesized that pharmacological inhibition of FOXP3 by systemically delivered, unformulated constrained ethyl-modified antisense oligonucleotides could modulate the activity of Tregs and augment antitumor immunity providing therapeutic benefit in cancer models and potentially in man.

Methods We have identified murine Foxp3 antisense oligonucleotides (ASOs) and clinical candidate human FOXP3 ASO AZD8701. Pharmacology and biological effects of FOXP3 inhibitors on Treg function and antitumor immunity were tested in cultured Tregs and mouse syngeneic tumor models. Experiments were controlled by vehicle and non-targeting control ASO groups as well as by use of multiple independent FOXP3 ASOs. Statistical significance of biological effects was evaluated by one or two-way analysis of variance with multiple comparisons.

Results AZD8701 demonstrated a dose-dependent knockdown of FOXP3 in primary Tregs, reduction of suppressive function and efficient target downregulation in humanized mice at clinically relevant doses. Surrogate murine FOXP3 ASO, which efficiently downregulated Foxp3 messenger RNA and protein levels in primary Tregs, reduced Treg suppressive function in immune suppression assays in vitro. FOXP3 ASO promoted more than 70% reduction in FOXP3 levels in Tregs in vitro and in vivo, strongly modulated Treg effector molecules (eg, ICOS, CTLA-4, CD25 and 4-1BB), and augmented CD8⁺ T cell activation and produced antitumor activity in syngeneic tumor models. The combination of FOXP3 ASOs with immune checkpoint blockade further enhanced antitumor efficacy.

Conclusions Antisense inhibitors of FOXP3 offer a promising novel cancer immunotherapy approach. AZD8701 is being developed clinically as a first-in-class

FOXP3 inhibitor for the treatment of cancer currently in Ph1a/b clinical trial (NCT04504669).

INTRODUCTION

Regulatory T cells (Tregs) play critical roles in promoting immunologic self-tolerance and immune homeostasis by suppressing aberrant or excessive immune responses to self-antigens and pathogens.^{1 2} However, as critical as Tregs are to the maintenance of immune homeostasis, they pose a barrier in mounting an effective host response to tumor cells.³ Consistent with this, intratumoral Tregs may contribute to a poor prognosis in several cancers.^{4–8} In addition, the suppressive function of Tregs can also dampen the efficacy of several anticancer immunotherapies^{9–11} suggesting that therapies capable of selectively inhibiting Treg function would be promising additions to the cancer immunotherapy arsenal.

The forkhead-box family transcription factor FOXP3 is the key driver of the gene expression program underlying the immune suppressive function of Tregs.^{12 13} Mutations to the gene encoding FOXP3 lead to fatal autoimmune disorders in both mice and human patients with immune dysregulation, polyendocrinopathy, enteropathy, X-linked syndrome, confirming the critical role of this factor in regulating the immunosuppressive properties of Tregs.¹⁴ In preclinical tumor models, transient genetic depletion of FOXP3 in Tregs improves effectiveness of therapeutic vaccination against established melanoma tumors suggesting FOXP3 may be

a highly attractive target for cancer immunotherapy.^{15 16} However, transcription factors such as FOXP3 are notoriously difficult to target with conventional therapeutic modalities and are often considered undruggable.

Therapeutic nucleic acid-based approaches, including antisense oligonucleotides (ASOs), offer the potential to yield drugs, based on gene sequence information alone, for targets that have proven to be intractable to alternative drug modalities.^{17 18} ASOs are short synthetic single-stranded nucleotide polymers that selectively bind to a target RNA through Watson-Crick base pairing and, based on the ASO chemistries employed, can be designed to (i) recruit the cellular enzyme RNase H1 leading to the catalytic destruction of the target RNA, or (ii) alter the processing (eg, splicing) of their RNA targets.^{18 19} Generation 2.0 ASOs have common chemical and biological properties, are generally safe and well-tolerated in the clinic leading to several recent new drug approvals including Tegsedi, Waylivra and the blockbuster drug Sprinraza, for the treatment of patients with the devastating neurodegenerative disease spinal muscular atrophy.^{17 19 20}

Continued efforts to improve the stability and potency of ASOs have resulted in the discovery of a class of ASOs that employ 2'-4' constrained ethyl (cEt) residues and exhibit significantly enhanced in vitro and in vivo potency compared with earlier generation ASO molecules.^{21 22} More recently, these cEt-containing ASOs targeted to previously undruggable tumor cell targets have shown therapeutic promise for the treatment of cancer.²²⁻²⁴

In this work we optimized and characterized ASOs targeting the Treg lineage-defining transcription factor FOXP3 in mouse preclinical models and in human primary Tregs. These studies ultimately support the development of a human FOXP3 inhibitor and selection of AZD8701 as the first-in-class human clinical candidate ASO inhibitor of FOXP3 for the treatment of cancer.

MATERIALS AND METHODS

Additional Materials and Methods can be found in online supplemental materials.

Mice and in vivo tumor studies

BALB/c mice were purchased from Envigo, Shanghai Lingchang Bio-Technology or Charles River and female C57BL/6 mice were purchased from Charles River or The Jackson Laboratory and housed under specific pathogen-free conditions. All procedures were carried out in accordance with UK home office (local) regulations and with approved institutional guidelines. Studies run at Ionis Pharmaceuticals or CrownBio were performed in accordance with the guidelines established by the internal Institutional Animal Care and Use Committee. Mice were housed under pathogen-free conditions in individually ventilated cages under controlled conditions of temperature (19°C–23°C), humidity (55%±10%), photoperiod (12 hours light/12 hours dark), air exchange with food

and water provided ad libitum. All animal manipulations were conducted in a biosafety cabinet maintained under positive pressure. The Ionis Pharmaceuticals facilities have been accredited by Assessment and Accreditation of Laboratory Animal Care.

ID8-VEGF (3–5×10⁶ cells/mouse), A20 (3×10⁵–1×10⁷ cells/mouse), MC-38 (1×10⁷ cells/mouse) tumor cells were implanted subcutaneously (s.c.) in the left flank of syngeneic mice. 4T1 (1×10⁴ cells/mouse) were implanted in mammary fat pads of female BALB/c mice. Twelve days before (MC-38 and 4T1) or 1 day after (A20 and ID8-VEGF) implantation, mice were randomized into groups by body weight and dosed s.c. with FOXP3 ASOs 895310, 895317 or control ASO 792169 in phosphate buffered saline (PBS) or intraperitoneally with anti-programmed cell death 1 (PD-1) (BioXcell, RMP1-14, rat IgG2a) or anti-programmed cell death ligand 1 (PD-L1) (mouse IgG1, clone D265A; AstraZeneca). Tumor volumes were calculated using the following formula based on caliper measurements of length (l) and width (w): volume=(pi/6)×l×w.²

For downstream flow cytometric experiments, cells were liberated from tumors using a mouse tumor dissociation kit and tissue dissociator (Miltenyi) according to the manufacturer's instructions.

For non-tumor bearing studies, BALB/c female mice were dosed s.c. 2–5 times per week with 20 or 50 mg/kg FOXP3 ASOs 895310, 895317 or control ASO 792169 in PBS for 4–6 weeks. At the end of each week, whole blood (cardiac puncture, under terminal isoflurane anesthesia) and spleens were removed and processed for flow cytometry, the remaining carcass was submerged into 10% buffered formalin and certain tissues were processed for histological analysis.

Humanized mice

Female NOD.Cg-Prkdcscid Il2rgtm1Wjl/SzJ (NSG) mice were implanted with 1×10⁷ human peripheral blood mononuclear cells (PBMC) per mouse (JAX). Seven days post PBMC implantation, humanized mice were s.c. treated with indicated doses of ASOs for four consecutive days. Spleens were harvested 24 hours after the last dose and processed for RNA isolation and flow cytometry analysis.

Human CD4 cells were isolated from splenocytes of humanized PBMC mice by the combination of negative magnetic purification steps using a mouse and human EasySep CD4 T cell purification kits (Stemcell Technologies). Purified human CD4 cells were cultured in ImmunoCult-XT T cell expansion media (Stemcell Technologies) supplemented with 30 ng/mL of human recombinant interleukin (IL)-2 (Stemcell Technologies). CD4 cells were treated ex vivo with oligonucleotides by free uptake in a dose-response study for 72 hours. Cells were activated for 24 hours in the presence of ImmunoCult human CD3/CD28/CD2 T cell activator (Stemcell Technologies). Cells were collected and evaluated for changes

in the levels of FOXP3 messenger RNA (mRNA) by RT-qPCR and levels of FOXP3 protein by flow cytometry.

ASOs

All ASOs used in this study were 16 nucleotides in length, connected sequentially by phosphorothioate internucleoside linkages. The three nucleotides at both the 5' and 3' ends are composed of 2'-4' cEt-modified ribonucleotides, which confer an increased affinity to the target mRNA and increased resistance to exo and endonucleases within the cell.²⁰ The central portion is composed of 10 deoxynucleotides, enabling RNase H1 to recognize and cleave the target mRNA in the ASO:RNA duplex. The sequence of the human FOXP3 lead ASO AZD8701/IONIS-1063734 was GATTTTGACATTCTGC. The sequences of the mouse FOXP3 ASOs used in this study were ION-895310 (ATATGTATAGCTGGTT), ION-895317 (GTAATATTAGGATGG), ION-895545 (TAGCATGTAGTACAGG) and ION-895562 (TAGTTTTGGGTTGAGG). The simple letters indicate DNA and the italicized/underlined letters indicate cEt-modified RNA bases.

Statistics

Error bars relate to SEM unless indicated in figure legends. Appropriate statistical testing was performed using GraphPad Prism (V.7 or V.8). Statistical significance is indicated as follows: * $p \leq 0.05$, ** $p \leq 0.01$, *** $p \leq 0.001$, **** $p \leq 0.0001$.

RESULTS

AZD8701 potently reduces FOXP3 expression in vitro and in vivo, reversing human Treg immunosuppressive function in primary cells

To identify the most potent human FOXP3 ASOs approximately 2500 compounds were screened in FOXP3-expressing anaplastic cell lymphoma line SUPM2 in vitro. Approximately 100 of the most effective FOXP3 ASOs selected from this primary screen were evaluated for potency in dose-response experiments in SUPM2 cells (online supplemental figure 1A), in primary Tregs isolated from humanized mice (online supplemental figure 1B) or human PBMCs (online supplemental figure 1C). The most potent and selective FOXP3 ASOs were further evaluated for activity in vivo versus human Tregs in humanized PBMC mice. Several ASOs produced significant reductions of FOXP3 mRNA and protein in human Tregs in humanized PBMC mice (online supplemental figure 1D). AZD8701 emerged as the best human FOXP3 antisense inhibitor, with robust activity in primary human Tregs in vitro and Tregs in humanized PBMC mice in vivo as well as acceptable tolerability profiles in rodents and non-human primates. Structurally, AZD8701 binds to the intronic site on FOXP3 pre-mRNA which is present in all known FOXP3 RNA isoforms (online supplemental figure 1E).

AZD8701 showed potent dose-dependent FOXP3 protein knockdown in primary human Tregs ($65.2 \text{ nM} \pm 6.7 \text{ SEM}$, range 44–78 nM in six donors), and was highly efficacious,

with doses $>1 \mu\text{M}$ promoting near-complete extinction of target protein expression (figure 1A,B). AZD8701 downregulated the expression of canonical FOXP3 targets CTLA4, ICOS, GITR and CCR8 at $1 \mu\text{M}$ dose (figure 1C), and in a dose-dependent manner (online supplemental figure 2A). We evaluated the relationship between FOXP3 knockdown and modulation of downstream pharmacodynamic biomarkers in a range of in vitro Treg samples treated with multiple FOXP3 ASOs at different concentrations. Correlation analysis corroborated the relationship between FOXP3 modulation and CTLA4, ICOS, GITR, CCR8 but not CD3 expression in primary Tregs (online supplemental figure 2B). AZD8701 strongly reduced FOXP3 protein expression in thymic natural Tregs (nTreg) and effector Tregs (eTreg) subsets, defined by CD45RA and FOXP3 expression in PBMCs from healthy donors (figure 1D,E). FOXP3 can be transiently expressed at low levels in conventional T cells but without showing immunosuppressive activity.^{25 26} Some recent data suggest that FOXP3 expression on CD8⁺ T cells is an early and tumor-related event that may limit anti-tumor efficacy.²⁷ We also detected FOXP3 expression in in vitro-stimulated human PBMCs and stimulated CD4⁺ and CD8⁺ conventional T cells (online supplemental figure 2C). Furthermore, FOXP3 ASOs with potency similar to AZD8701 modulated a wider 96-gene expression signature of immune-related genes and including canonical FOXP3 target genes (online supplemental figure 3).

Intratumoral Treg conversion from dominant conventional T cells (Tconv) may have a major impact on the tumor microenvironment (TME). Treg enrichment may result from the expansion of nTreg, but also through the conversion of Tconv into induced Treg (iTreg) under antigen stimulation or tumor-suppressive conditions. Tumor cells can secrete tumor growth factor β (TGF- β) that may directly or indirectly induce naïve T cell conversion to FOXP3⁺ iTregs.²⁸ AZD8701 reduced human iTreg functions in suppression assays in vitro (figure 1F,G). In vivo, AZD8701 promoted dose-dependent FOXP3 knockdown, an essential parameter for a potential therapeutic agent. When administered to mice engrafted with human PBMCs (humanized mice) (figure 1H), AZD8701 inhibited FOXP3 mRNA (figure 1I) and promoted significant downregulation of FOXP3 protein levels in splenic, blood and bone marrow Tregs (figure 1J). Together, these data show AZD8701 drives dose-dependent modulation of FOXP3 expression, changes in downstream FOXP3-dependent immunosuppressive biomarker expression, reduction of Treg suppressive function ex vivo and FOXP3 knockdown in vivo at clinically achievable doses.

Pharmacological targeting of murine FOXP3 in vivo results in immune activation without promoting overt autoimmunity

To further explore the pharmacology of FOXP3 ASOs, mouse surrogate ASOs with equivalent potency and tolerability to AZD8701 were used to investigate the consequences of modulating Tregs and other immune markers in vitro, and in peripheral tissues and tumors in vivo. We first determined the ability of cEt-modified ASOs to

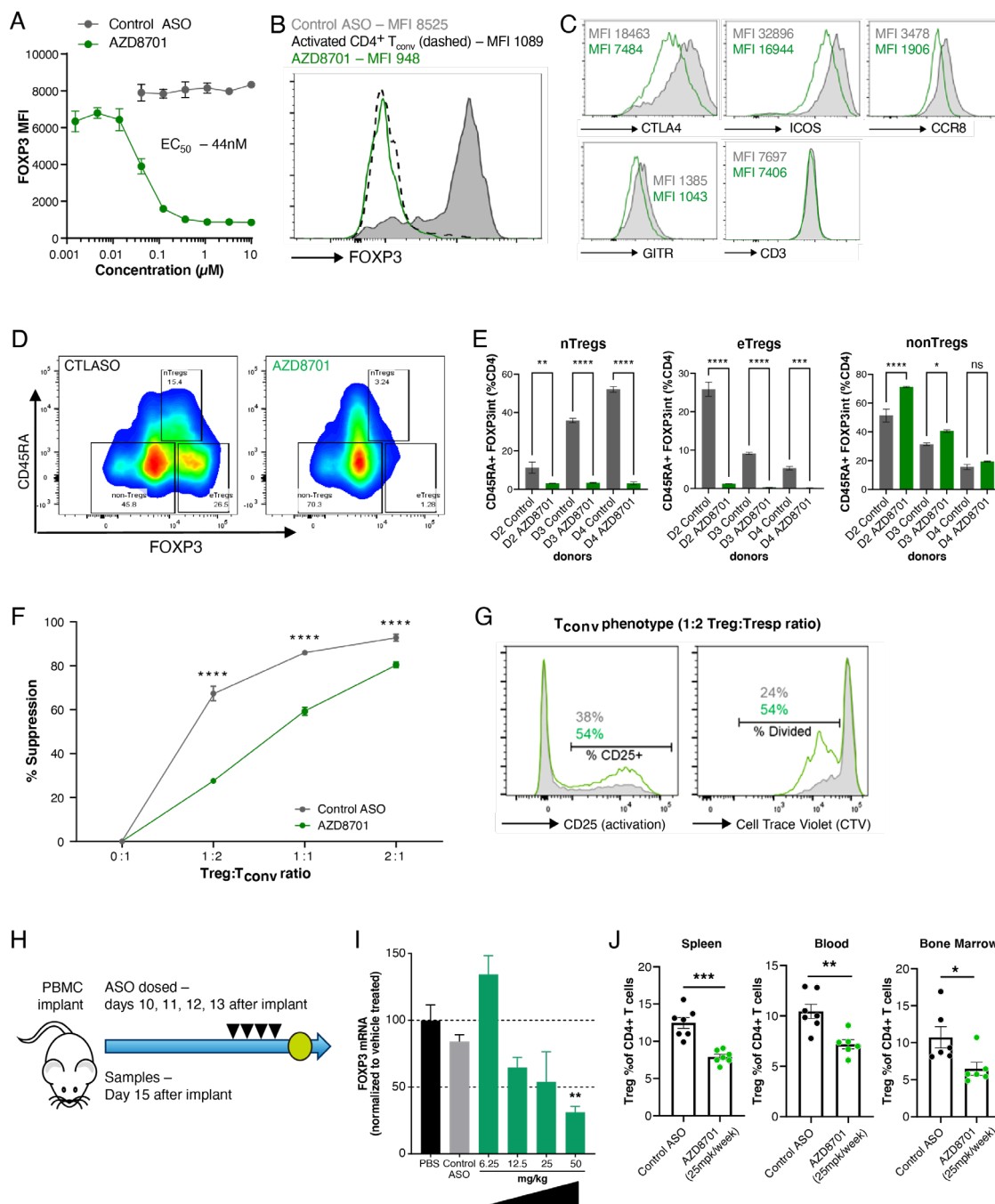


Figure 1 AZD8701 is a highly potent clinical candidate ASO targeting human FOXP3. (A–C) Primary human Tregs were isolated from human PBMCs and cultured with AZD8701 or control ASO in duplicates for a total of 9 days, in the presence of Dynabeads human T-activated CD3/CD28 for the final 2 days of culture. (A) Line graph and (B) histogram show FOXP3 protein abundance in cultured Tregs as measured by flow cytometry. Histogram shows representative data for Tregs cultured with 1 μM ASO. (C) Histograms show the abundance of indicated proteins from a representative treatment with 1 μM AZD8701. (D–E) Contour plot and quantification of FOXP3 knockdown in human PBMC nTregs and eTregs with AZD8701 by flow cytometry. Data shown for three healthy donors. (F–G) iTregs were differentiated and cultured in the presence of ASOs in quadruplicates. Data represent ≥ 3 independent experiments and a total of ≥ 6 independent donors. (F) Line graph shows ability of iTregs to inhibit proliferation of effector cells in an in vitro suppression assay. (G) Histograms show representative CD25 or CellTrace Violet (CTV) staining on effector cells cultured at a 1:2 iTreg:Teffector ratio. (H) NSG mice were humanized by the infusion of human PBMC and treated systemically for four consecutive days with different AZD8701 doses. (I) FOXP3 messenger RNA expression was quantified by RT-qPCR. $N=4$ per group. (J) FOXP3 protein levels were quantified by flow cytometry in spleen, blood and bone marrow of humanized mice treated as in (F). $N=7$ per group. Data in figure is representative of ≥ 2 independent experiments. Error bars are $\pm\text{SEM}$ *, $p \leq 0.05$; **, $p \leq 0.01$; ***, $p \leq 0.001$; ****, $p \leq 0.0001$ by one-way analysis of variance (ANOVA) with Dunnett's post-test for E and J and two-way ANOVA with Dunnett's post-test for F. Differences are calculated relative to control ASO (E, F and J) or saline (I). ASOs, antisense oligonucleotides; eTreg, effector Tregs; iTreg, inducible Tregs; nTreg, natural Tregs; PBS, phosphate buffered saline; Treg, regulatory T cells.

reduce Foxp3 mRNA in primary murine Tregs in vitro. Tregs were expanded in mice in vivo by injection of IL-2-anti-IL-2 antibody complex²⁹ and total Treg-enriched CD4 T cells were purified from spleen and treated with a panel of murine Foxp3 ASOs for 72 hours. FOXP3 ASOs produced robust dose-dependent inhibition of FOXP3 mRNA expression in primary murine Tregs with the most potent ASOs demonstrating IC₅₀ values between 0.1 and 0.2 μ M (online supplemental figure 4A,B).

Two mouse FOXP3 ASOs (895562 and 895545) were selected as they effectively downregulated FOXP3 in primary Tregs isolated from spleens of unmanipulated WT mice. Culturing Tregs in the presence of FOXP3 ASOs (5 μ M) for 7 days promoted >75% reduction in FOXP3 mRNA and protein (figure 2A). To evaluate whether FOXP3 knockdown also modulated a wider immunosuppressive gene expression profile in murine Treg, we examined a subset of previously characterized Treg signature genes, revealing downregulation of several downstream suppressive genes (figure 2B).^{30–32} Moreover, protein expression of the canonical FOXP3 targets CTLA4, CD25, GITR and CD73 were also downregulated with FOXP3 ASO treatment (figure 2C). FOXP3 ASOs could also reverse immunosuppressive Treg functions in suppression assays in vitro. iTregs were differentiated from naïve CD4 T cells in the presence of FOXP3 or control ASOs. Naïve T cells were then activated with soluble α CD3 and B-cell APCs in the presence of the iTregs. While iTregs cultured in the presence of control ASOs maintained an ability to suppress effector T cell (Teff) proliferation, FOXP3 ASO treatment abrogated iTreg suppressive capability (figure 2D). Consistent with the human FOXP3 ASOs, mouse FOXP3 ASOs can target FOXP3 RNA for degradation, resulting in loss of Treg suppressive phenotypes and functions in vitro.

Next, we characterized the pharmacology of murine FOXP3 ASO in Tregs in vivo and the consequences of ASO-mediated FOXP3 inhibition in normal mice. Murine FOXP3 ASOs with optimal in vivo properties, for example, activity and tolerability, were identified from a set of 20 FOXP3 ASOs that produced the best pharmacology in Tregs in vitro (online supplemental figure 4B). Mice were systemically treated with FOXP3 ASOs for 3 weeks. Murine FOXP3 ASOs 895310 and 895317 emerged as the most well-tolerated compounds in vivo and they produced significant Foxp3 mRNA knockdown in preliminary single-dose studies (figure 3A). When benchmarked to previous tool compounds in vitro, 895310 and 895317 were equipotent inhibitors of FOXP3 protein induction in iTregs (figure 3B). Moreover, both compounds were active in primary nTregs, isolated directly from murine spleens (figure 3C).

We next characterized the kinetics of FOXP3 target engagement in vivo. FOXP3 ASOs were formulated in PBS and administered two times per week (BIW) via s.c. injection to WT mice, resulting in a progressive decrease in FOXP3⁺ Treg cell frequencies in the spleen (figure 3D). Benoist and colleagues recently described mouse models harboring loss-of-function (LoF) mutations in Foxp3,

which exhibit elevated expression of the exhaustion/activation biomarker PD-1 in the regulatory T-cell compartment.³³ Consistent with this, PD-1 induction on the residual FOXP3⁺ cells was detected in FOXP3 ASO-treated mice (figure 3E), suggesting a potential loss of Treg suppressive functions conferred by FOXP3 ASOs in vivo. Consistent with this, treated mice also expanded CD4⁺ and CD8⁺ lineage cells that were CD62l^{lo}CD44^{hi}, resembling Teffector/memory (Tem) cells (figure 3F). The early activation marker CD69 was induced on T-cells following FOXP3 ASO administration, suggesting that enhanced steady-state activation may underlie elevated Tem phenotypes (figure 3G). Importantly, the immune cell differentiation and in particular the immunopotentiating phenotypes conferred by mouse FOXP3 ASO administration were reversible. WT mice were dosed with FOXP3 ASO for 3 weeks, and FOXP3⁺ Treg and CD69⁺/Tem population frequencies were tracked by flow cytometry after cessation of dosing, revealing a return of FOXP3⁺ Treg population to baseline levels followed by normalization of CD69⁺/Tem population frequencies within 2 weeks after the last ASO dose (figure 3H).

Genetic or induced ablation of FOXP3 results in profound autoimmune manifestations and rapid death in mice,^{13 34} while transient/partial Treg depletion is well-tolerated.³⁵ Similarly, partial LoF FOXP3 mutations are associated with minor inflammatory manifestations with a late onset (>35 weeks of age).³³ To evaluate whether FOXP3 ASOs promote immune-related phenotypes or toxicities, mice were treated with FOXP3 ASOs for an extended chronic time course.^{12 13} FOXP3 ASO administration was not associated with clinical signs, nor did we observe body weight reductions over >35 days of treatment (online supplemental figure 5A). While FOXP3 deficient mice and patients are typified by elevated circulating cytokines,^{13 36} no histopathological findings associated with autoimmunity (online supplemental figure 5B) and negligible cytokine elevation was observed in plasma up to 12 weeks of mouse FOXP3 ASO dosing (online supplemental figure 5C). Moreover, no unexpected inflammatory responses or differential serum antibody production was observed following an acute vaccine challenge in FOXP3 ASO-treated mice (online supplemental figure 5D). Together, these results demonstrate that FOXP3 ASOs can titrate Treg FOXP3 levels to enhance immunopotentiating phenotypes in a reversible manner and are not associated with overt autoimmune/inflammatory manifestations.

Foxp3 ASOs promote antitumor effects in vivo as a monotherapy or in combination with immune checkpoint blockade

Having established that human and murine FOXP3 ASOs were able to reduce FOXP3 expression in Tregs, decreasing Treg-mediated immunosuppression, we hypothesized that FOXP3 ASOs would modulate Treg function in the TME. Mice bearing syngeneic tumors were treated with murine FOXP3 ASOs to reduce FOXP3 expression in intratumoral Tregs and modulate antitumor immunity. By flow cytometry, we confirmed that the majority of the FOXP3+

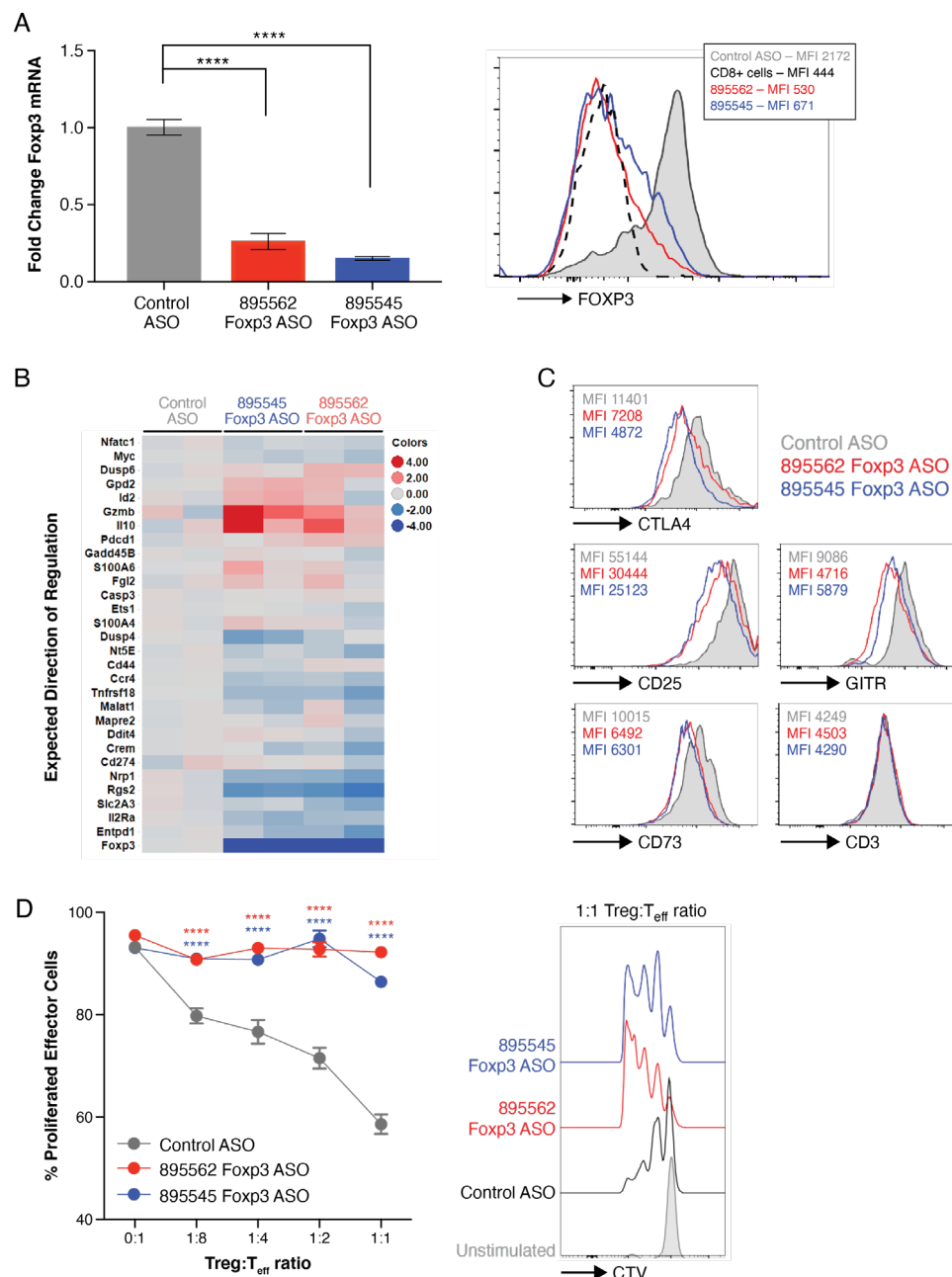


Figure 2 Antisense-mediated knockdown of mouse FOXP3 promotes loss of Treg suppressive phenotypic markers and function. (A) Primary Tregs were isolated from mouse spleen and cultured with ASOs (5 μ M) in triplicates for 7 days. Bar chart shows relative FOXP3 mRNA expression measured by RT-qPCR, histogram shows FOXP3 protein expression measured by flow cytometry. (B) Inducible Tregs (iTregs) were differentiated and cultured in the presence of ASO for a total of 7 days. Heatmap shows expression of FOXP3-dependent mRNA genes as measured by Fluidigm. (C) Histograms show abundance of indicated proteins in primary Tregs. (D) iTregs were differentiated and cultured in the presence of ASOs and evaluated for their ability to inhibit proliferation of effector cells in an in vitro suppression assay in duplicates. Histograms show representative CellTrace Violet (CTV) staining on effector cells cultured at a 1:1 Treg:Teffector ratio. Data in figure represent ≥ 2 independent experiments. *, $P \leq 0.05$; **, $p \leq 0.01$; ***, $p \leq 0.001$; ****, $p \leq 0.0001$ by one-way analysis of variance (ANOVA) with Dunnett's post-test for (A) and two-way ANOVA with Dunnett's post-test for (D). Differences are calculated relative to control ASO. ASOs, antisense oligonucleotides; mRNA, messenger RNA; Tregs, regulatory T cells.

Tregs in the tumor were positive for a Treg-enriched surrogate marker Helios,³⁷ enabling assessment of the relative change in FOXP3 protein levels in these cells (figure 4A). Following treatment with FOXP3 ASO, the total fraction of Helios⁺ CD4 T cells was unchanged indicating a non-depleting mechanism. FOXP3 ASO treatment (with both

895310 and 895317) conferred up to 70% reduction in FOXP3 protein—in two different syngeneic models, ID8-VEGF and A20 (figure 4B) after 62 days and 24 days after implantation, respectively. Moreover, the growth of ID8-VEGF and A20 tumors was significantly attenuated in FOXP3 ASO-treated but not control ASO-treated animals

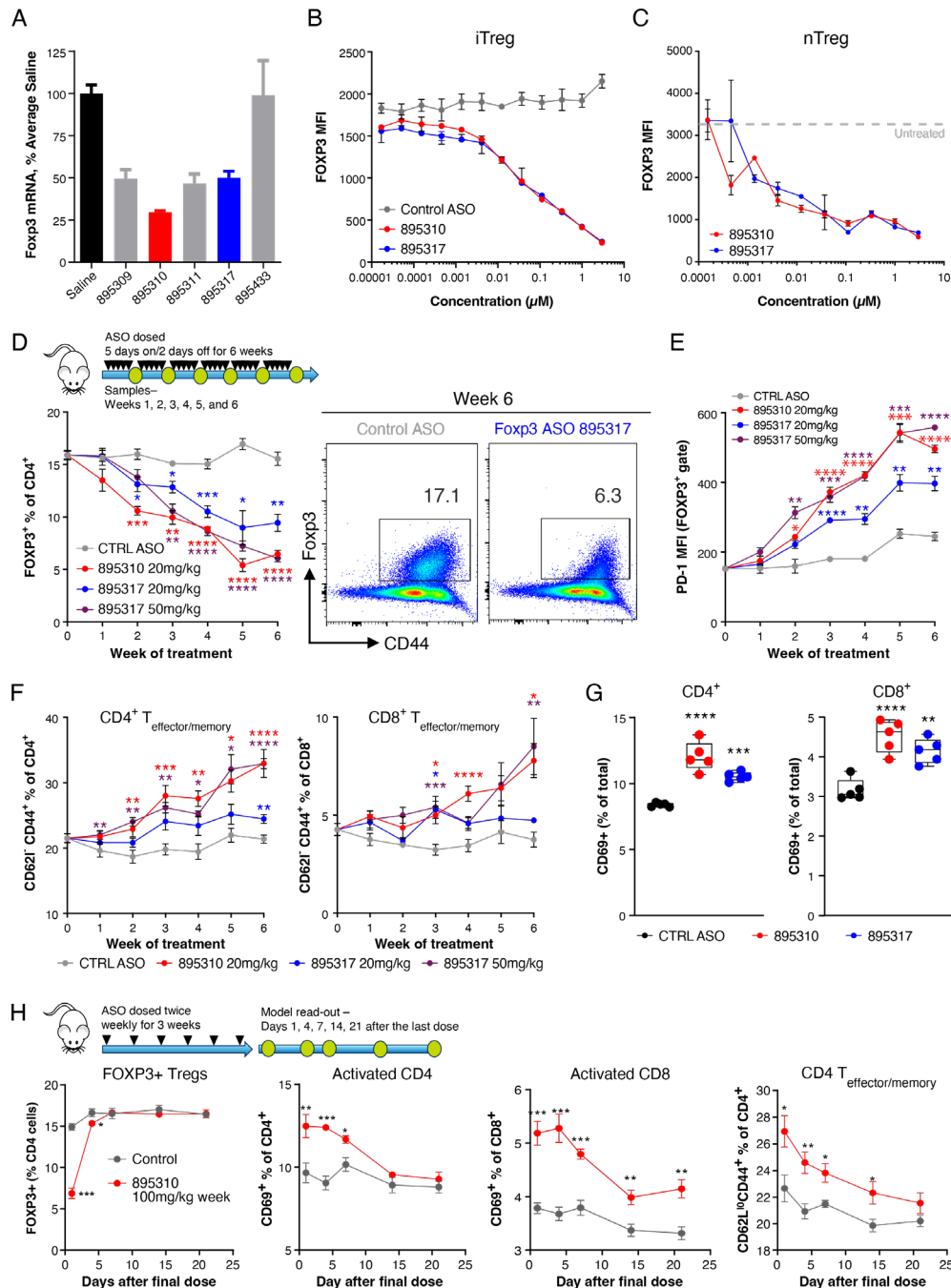


Figure 3 Mouse FOXP3 ASOs promote FOXP3 knockdown in vivo, which associates with phenotypes indicative of immunopotentiality. (A) Mice were systemically treated with FOXP3 ASOs for 3 weeks at 100 mg/kg/week dose. CD4⁺ T cells were isolated from spleens and FOXP3 messenger RNA was measured by RT-qPCR. ASOs selected for further in vivo evaluation are highlighted in red and blue. N=4 per group. (B) iTregs were differentiated in the presence of ASO in duplicates for 5 days, and FOXP3 protein abundance was measured by flow cytometry. (C) Primary splenic nTregs were cultured in the presence of indicated ASOs in duplicates for 7 days, and FOXP3 protein abundance was measured by flow cytometry. (D–G) 20 mg/kg and 50 mg/kg FOXP3 ASOs or 50 mg/kg control ASO were administered to BALB/c mice via subcutaneously route 5 days on 2 days off. N=5 per group. (D) The line graph shows the frequency of gated FOXP3⁺ cells within the splenic CD4⁺ population. Pseudocolor density plots show representative FOXP3⁺ gating. (E) Line graph shows programmed cell death 1 protein expression on detectable FOXP3⁺ cells. (F) Line graphs show the frequency of CD62L^{lo}CD44^{hi} T-memory cells within the total CD4⁺ T-cell population. (G) Scatter bar charts show the frequency of CD69⁺ cells within the CD4⁺ or CD8⁺ populations at the week six time point. (H) ASOs were dosed (100 mg/kg two times per week) for 3 weeks before spleens from cohorts of mice were analyzed by flow cytometry at indicated time points following cessation of treatment. N=5 per group. Data represent two independent experiments. Error bars are SEM data in figure represent ≥ 2 independent experiments. *, $P \leq 0.05$; **, $p \leq 0.01$; ***, $p \leq 0.001$; ****, $p \leq 0.0001$ by one-way analysis of variance (ANOVA) with Dunnett's post-test for (A and G) and two-way ANOVA with Dunnett's post-test for (D, E, F and H). Differences are calculated relative to control ASO (D–H) or saline (A). ASOs, antisense oligonucleotides; iTreg, inducible Tregs; nTreg, natural Tregs; Tregs, regulatory T cells.

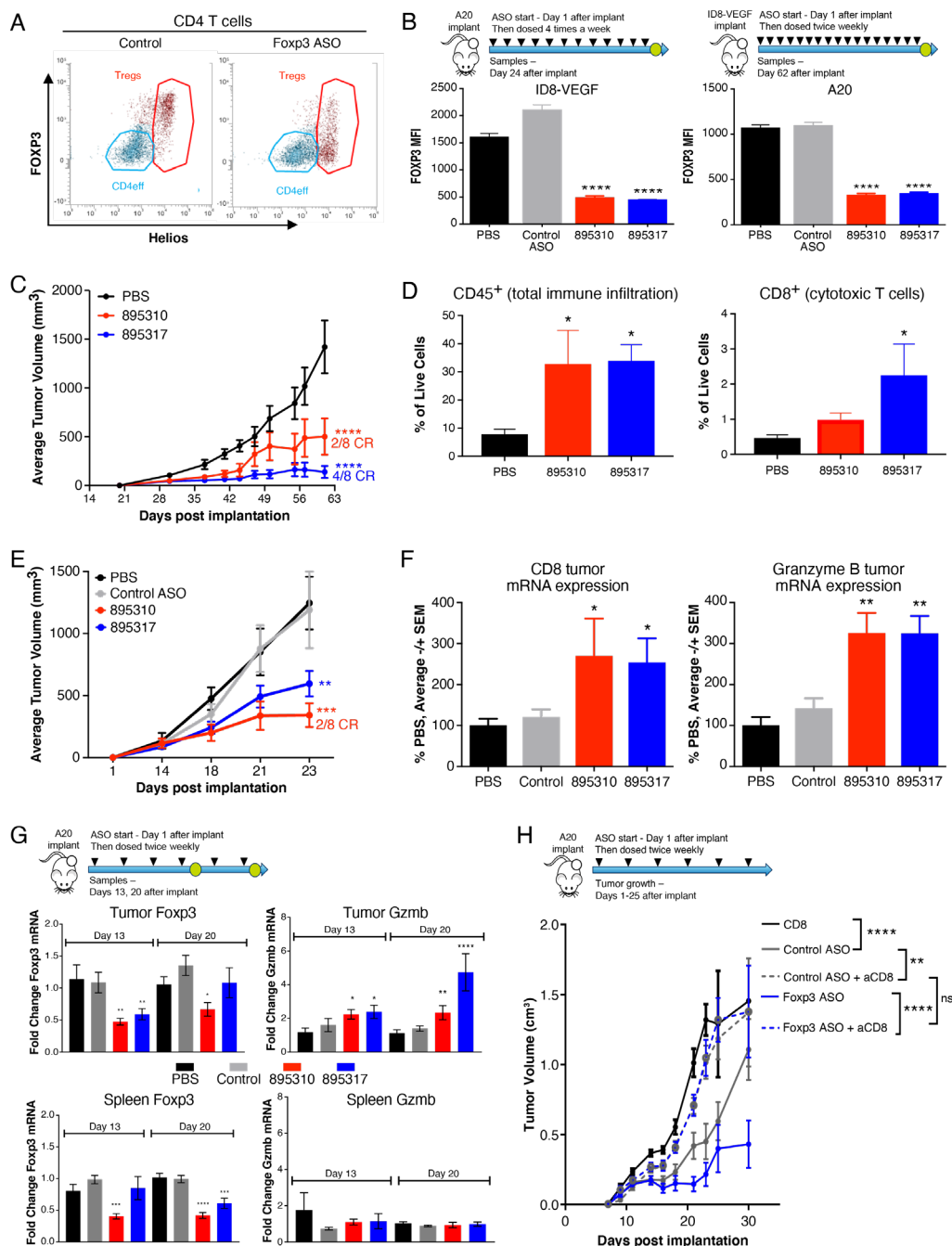


Figure 4 Single-agent antitumor efficacy mediated by mouse FOXP3 ASOs. (A–F) ID8-VEGF or A20 tumor-bearing mice were systemically treated with FOXP3 ASOs starting at day 1 after implant at 50 mg/kg BIW until day 62 (ID8-VEGF) or four times per week until day 24 (A20). N=8 per group. (A) Tumors were dissociated and tumor-infiltrating Tregs were analyzed by flow cytometry. Helios +CD4⁺ Tregs are shown in red. (B) FOXP3 protein expression was measured in Helios +CD4⁺ Tregs. Line graphs show (C) ID8-VEGF and (E) A20 tumor volumes. The number of complete responses (CR) vs total number of animals in the group is indicated next to lines. (D) ID8-VEGF tumors were dissociated, and abundance of total tumor-infiltrating leukocytes (CD45⁺ cells) and CTL (CD8⁺ T cells) were analyzed by flow cytometry. (F) Total RNA from A20 tumors was analyzed for the mRNA expression of CTL marker CD8 and immune cell activation marker Gzmb. (G) A20 tumor-bearing mice were treated with indicated ASO or vehicle control 50 mg/kg BIW and tumors analyzed by flow cytometry at day 13 or day 20 time points. N=10 per group. Bar charts show tumor or spleen Foxp3 and Gzmb expression measured by RT-qPCR. (H) CD8⁺ T cells were depleted in vivo with an α CD8 blocking antibody in A20 tumor-bearing mice that were treated with indicated ASO or control at 50 mg/kg BIW. N=12 per group. Data represent ≥ 4 independent experiments in (A–F), two independent experiments in (G) and a single cell depletion experiments in (H). *, $P \leq 0.05$; **, $p \leq 0.01$; ***, $p \leq 0.001$; ****, $p \leq 0.000$ by one-way analysis of variance (ANOVA) with Dunnett's post-test for (B, D, F and G) and two-way ANOVA with Dunnett's post-test for (C, E and H). Differences are calculated relative to PBS (B–G) or as indicated on the panel (H). ASOs, antisense oligonucleotides; BIW, two times per week; mRNA, messenger RNA; PBS, phosphate buffered saline; VEGF, vascular endothelial growth factor.

with 25%–50% of the animals achieving complete regressions (figure 4C,D,E). FOXP3 ASO treatment resulted in the marked increased recruitment of leukocytes (CD45⁺) and cytotoxic CD8⁺ T cells to the tumors in ID8-VEGF (figure 4D) and increased leukocyte cytotoxic marker GzmB in A20 model (figure 4F). Finally, to evaluate the kinetics of FOXP3 ASO-mediated antitumor immunity, we measured changes in inflammatory biomarkers in the A20 model at an early (day 13), and later (day 20) time point (figure 4G). We observed a progressive induction of GzmB expression, which preceded tumor growth inhibition, and was localized to the TME (figure 4G). Depletion of CD8⁺ T cells in vivo ablated FOXP3 ASO-mediated antitumor immunity (figure 4H). Collectively, these data suggested that inhibition of Treg immunosuppressive function through FOXP3 knockdown led to the enhancement of a highly specific T effector cell-mediated antitumor immune response.

Given the striking observations that mouse FOXP3 ASOs promote antitumor immunity and efficacy, we next evaluated the monotherapy efficacy of the FOXP3 ASOs in the A20 model with a dose-response to define a minimally efficacious dose in that preclinical model. We observed evidence for dose-dependent efficacy (online supplemental figure 6A) and FOXP3 knockdown in both tumors and spleen with coincident increase in CD4 effector T cell activation (online supplemental figure 6B,C). These data suggested that even relatively low doses of FOXP3 ASOs producing modest FOXP3 inhibition are sufficient to modify the TME and immune activation state to confer antitumor benefit in mice.

Next, we investigated the characteristics that may typify a FOXP3 ASO-sensitive tumor. The FOXP3 ASO sensitive ID8-VEGF and A20 tumors have a high accumulation of FOXP3⁺ Tregs in the TME as sensitive models.^{38,39} In contrast, models with low FOXP3⁺ Treg infiltrate in the TME (eg, 4T1 and MC-38) showed low sensitivity to FOXP3 inhibition (online supplemental figure 7). Despite the limited number of available models, the data support the hypothesis that FOXP3 positivity may predict which tumors have a greater likelihood of response to FOXP3 ASO administration.

Treg cells have been suggested to play a role in innate or acquired resistance to immunotherapy, and limit checkpoint inhibitor efficacy.^{10,11} In the A20 tumor model combination of mouse FOXP3 ASO with α PD-L1 significantly decreased tumor growth (figure 5A,B) and increased complete response (CR) rate compared with control groups and monotherapies (figure 5C). The combination promoted an increased infiltration of CD8⁺ T cells assessed by flow cytometry, and significant increase in dendritic cells in the TME in the FOXP3 ASO—treated arms (figure 5D). The changes in immune activation following treatment were systemic, with peripheral blood from treated mice exhibiting a significant increase in cytotoxic T cell and antigen presentation gene expression signatures (figure 5E).

To gain greater insight into the broader effects of reducing FOXP3 expression on CD4⁺ T cells we

performed a detailed analysis of the effects of FOXP3 ASO monotherapy and combination with α PD-L1 on CD4⁺ T cells in the TME by mass cytometry. Mice were treated with FOXP3 ASO and/or α PD-L1, and tumors collected for immunoprofiling at day 20 of treatment (figure 6A), time point preceding tumor regression when we had previously identified enhanced immune activation (figure 4G). T-distributed stochastic neighbor embedding (t-SNE) clustering showed significant changes in frequencies of different tumor CD4⁺ T cell populations (figure 6B) with a significant decrease in FOXP3^{hi}CD25^{hi} Tregs from 11.5% to 6.3% in the FOXP3 ASO group and 4.8% in the combination groups. The FOXP3^{lo}CD25^{lo} Treg fraction was significantly increased from 5.3% to 19.2% and 16.7% in the FOXP3 ASO and combination groups, respectively (figure 6C). Phenotypically, FOXP3^{lo}CD25^{lo} Tregs showed significantly less Ki67 expression and lower expression of Treg effector molecules such as GITR, LAG3, 4-1BB, CD25, OX40 and CTLA-4, which were driven primarily by the FOXP3 ASO and not α PD-L1 treatments (figure 6D,E). Taken together, these data support the mechanism of action of FOXP3 ASO in reprogramming Tregs into a low suppressive state in the TME, allowing us to dissect a discrete and complementary mechanism of action to α PD-L1 treatment.

PD-1 blockade monotherapy could lead to the skewing of the Teff/Treg balance in favor of Treg-mediated immunosuppression, limiting the response to immunotherapy.^{40,41} Therefore, we extended our work to evaluate mouse FOXP3 ASO efficacy in combination with α PD-1 immune checkpoint blocking antibodies in the A20 tumor model. FOXP3 ASOs promoted significant tumor growth inhibition, with CRs observed in a monotherapy arm, and increased the number of CR/near CR mice in combination with α PD-1 (figure 7A). In A20 tumor-bearing mice, α PD-1 immune checkpoint administration increased Foxp3 mRNA expression in tumors and spleens, which could be reduced by FOXP3 ASO coadministration (figure 7B,E). Foxp3 knockdown in the tumor was followed by increased CD8 T cell infiltration (figure 7C) and GzmB expression (figure 7D). These markers of cytotoxic activity were not observed in spleens (figure 7F,G), supporting previously observed non-systemic T cell activation. Thus, Tregs may represent a non-redundant or non-overlapping immunosuppressive mechanism in tumors that may complement immune checkpoint therapies. When taken together, these data represent a preclinical proof-of-concept that cEt-modified ASOs can efficiently target FOXP3 expression in Tregs, reduce their immunosuppressive phenotype in vivo, and promote antitumor immunity (figure 7H). This mechanism is novel, as it is not cyto-depletive, and can be modulated both by dose and kinetics to dynamically regulate the reversal of Treg suppressive function.

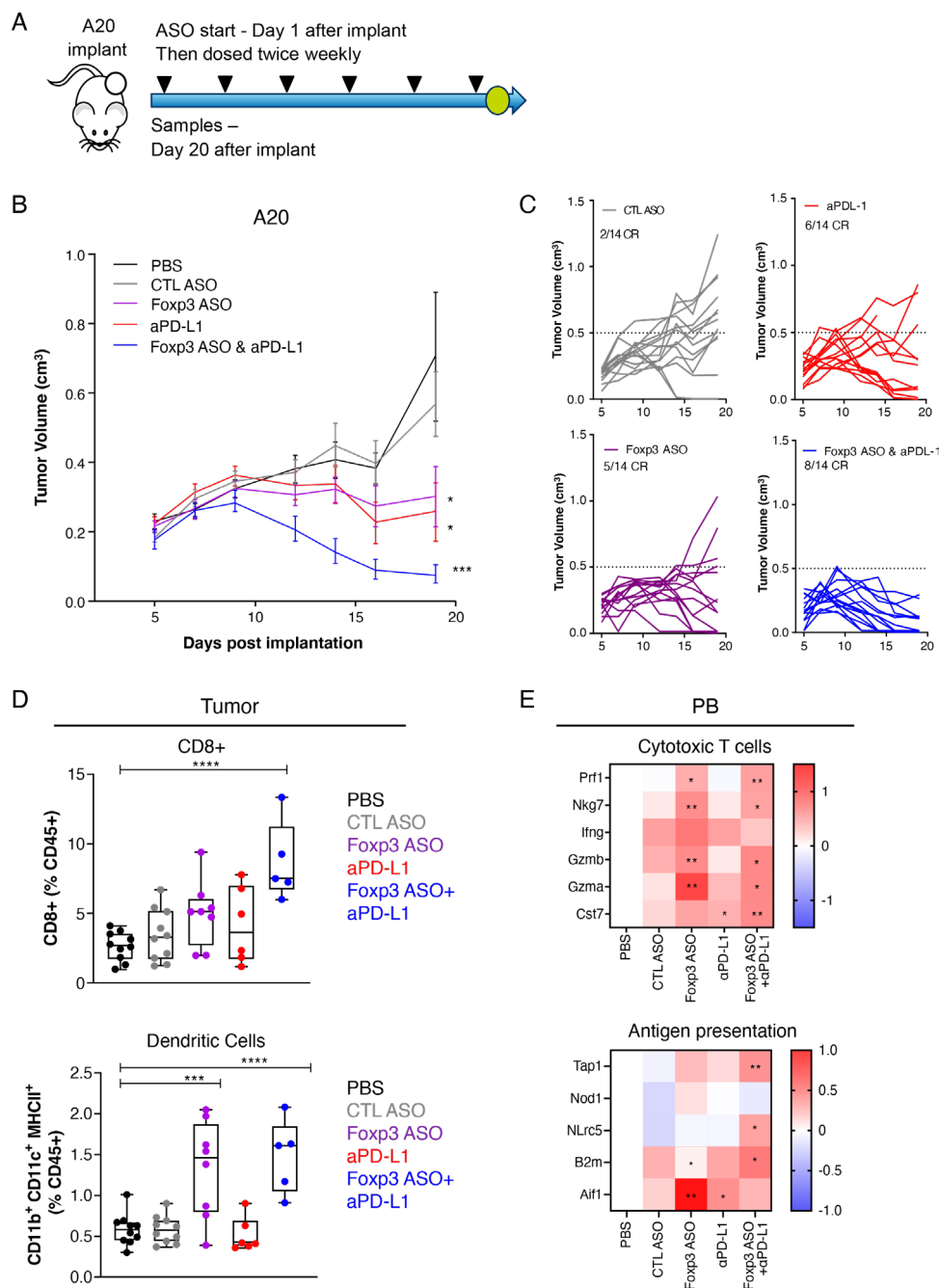


Figure 5 FOXP3 ASOs promote antitumor efficacy when combined with α PD-L1 immune checkpoint blockade. (A) Mice were treated with mouse FOXP3 ASO (895317) (50 mg/kg BIW) and α PD-L1 (10 mg/kg BIW) alone or in combination from day 1 post A20 tumor-implantation and dosed two times per week for the duration of the experiment. N=14 per group. (B) Mean tumor and (C) individual tumor volumes and indicated number of complete responses (CR). (D-E) Tumor samples and peripheral blood (PB) were analyzed at day 20 by flow cytometry and RNA levels, respectively. (D) Frequency of CD8⁺ T cells and dendritic cells in tumor and (E) cytotoxic T cell and antigen-presenting cell gene markers in PB. *, $P \leq 0.05$; **, $p \leq 0.01$; ***, $p \leq 0.001$; ****, $p \leq 0.0001$ by one-way analysis of variance (ANOVA) with Dunnett's post-test for (D and E) and two-way ANOVA with Dunnett's post-test for (B). Differences are calculated relative to PBS. ASOs, antisense oligonucleotides; BIW, two times per week; PBS, phosphate buffered saline; PD-1, programmed cell death 1; PD-L1, programmed cell death ligand 1.

DISCUSSION

Even in cases where the molecular pathogenesis underlying disease states is well defined, the discovery of effective therapeutic treatments often remains unrealized. In part, this reflects the fact that only approximately 20% of all human genes are thought to be members of what are

considered 'druggable' protein families.⁴² Thus, there is a tremendous need to develop technologies to expand the druggable fraction of the genome to treat disease more effectively.

In this study, we demonstrate that antisense technology, and in particular cEt chemistry ASOs, can be effectively

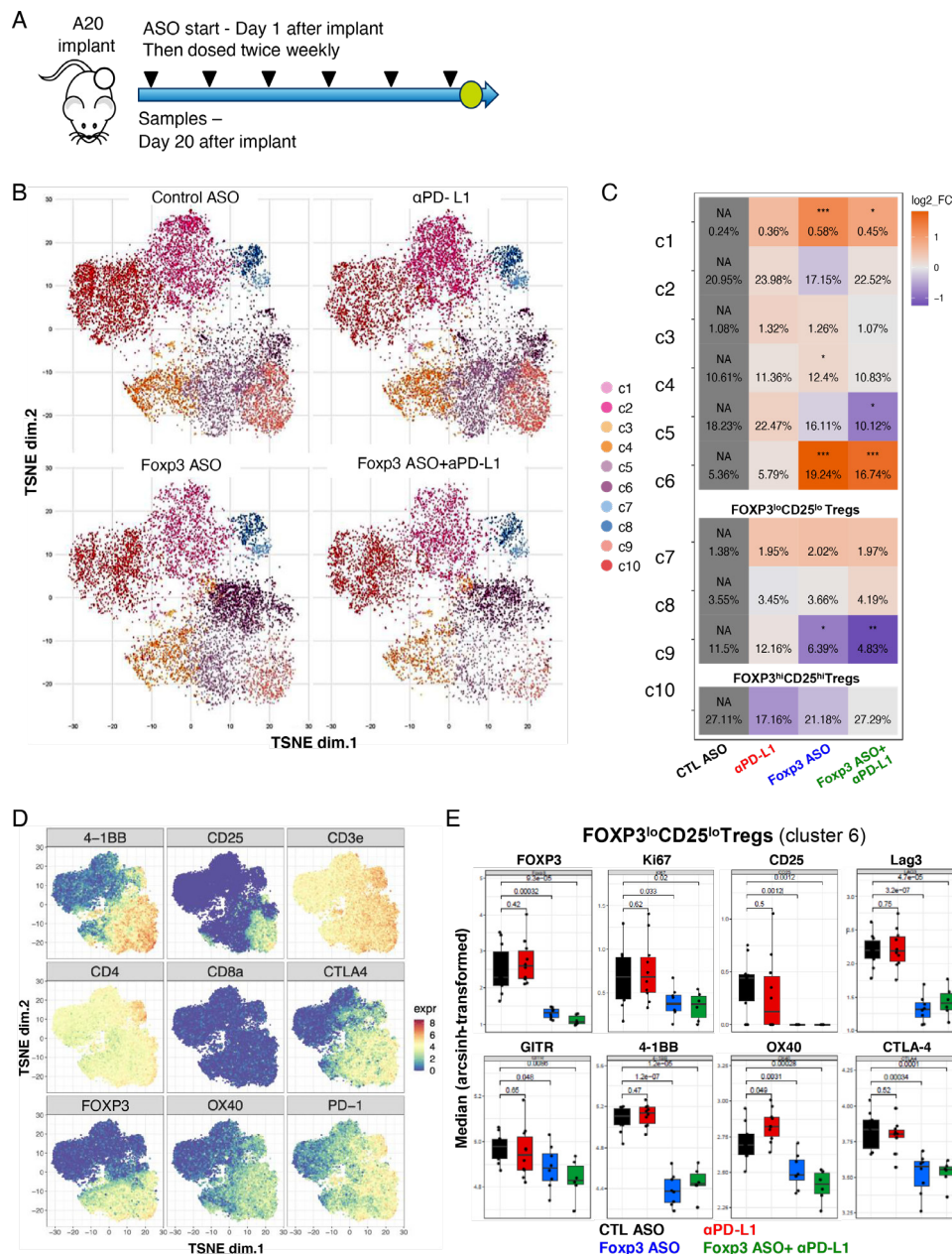


Figure 6 FOXP3 ASOs reprogram Treg effector cell phenotype in vivo in combination with α PD-L1 immune checkpoint blockade. (A) Mice were treated with ASO (50 mg/kg BIW) and α PD-L1 (10 mg/kg BIW) alone or in combination from day 1 post A20 tumor-implantation. N=14 per group. Tumors were analyzed by mass cytometry at day 20 after implantation. (B) t-SNE analysis of tumor-infiltrating CD4⁺ T cells. (C) Relative changes of CD4⁺ T cell clusters compared with control group. (D) Expression map of T cells and Tregs markers. (E) Quantification of Treg activation expression markers. Error bars are SD. *, p<0.05; **, p<0.01; ***, p<0.001; ****, p<0.0001 by one-way analysis of variance with Dunnett's post-test relative to control ASO. ASOs, antisense oligonucleotides; BIW, two times per week; t-SNE, t-distributed stochastic neighbor embedding; PD-L1, programmed cell death ligand 1; Treg, Regulatory T cells.

deployed to target difficult-to-drug proteins in immune cells including Tregs. Tregs have been long associated with immunosuppression in the TME and the clear association between FOXP3 and Treg immunosuppressive activity provided a known yet previously undruggable target for ASO technology. We have shown that treatment with murine FOXP3 ASOs resulted in monotherapeutic antitumor activity and combination benefit with either α PD-1 or α PD-L1 checkpoint blockade. Profiling of FOXP3 ASO efficacy across a range of discrete tumor

models revealed that antitumor efficacy was linked to a high Treg infiltration within the TME, and consequently it may be interesting to investigate whether there is an association between FOXP3 levels and clinical activity for such agents.

The discovery of the human FOXP3 ASO inhibitor AZD8701 opens a novel opportunity to selectively target Treg immunosuppressive function. Several drugs possessing a Treg-depletion mechanism of action have entered early phase clinical development, such

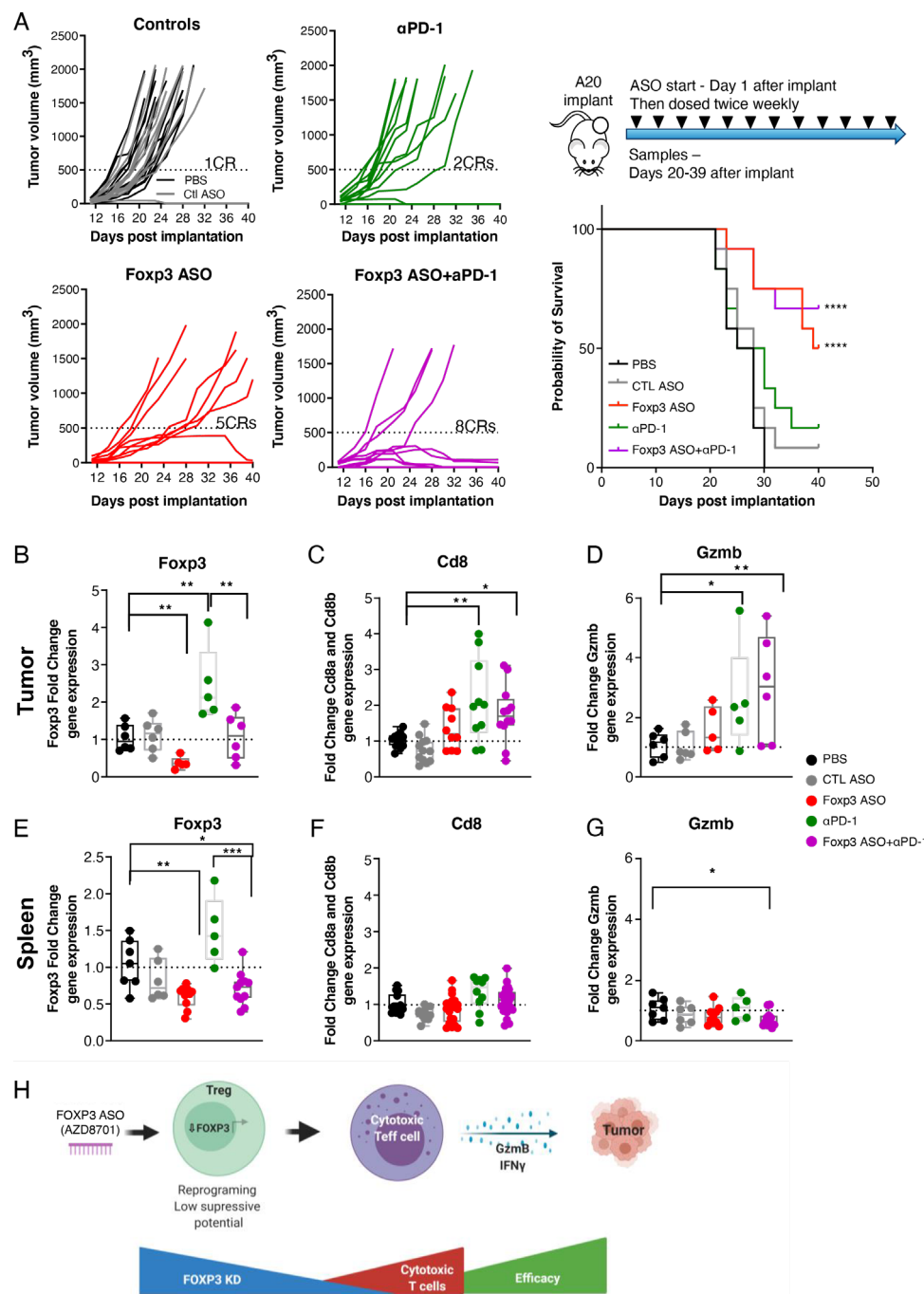


Figure 7 FOXP3 ASOs promote additive efficacy when combined with α PD-1 immune checkpoint blockade. Mice were treated with ASO 895310 (50 mg/kg BIW) and α PD-1 (10 mg/kg BIW) alone or in combination from day 1 post A20 tumor-implantation. ASO was dosed for the duration of the study. α PD-1 was dosed six times. N=12 per group. Mice were sacrificed when tumors exceeded 1500 mm³ or after 40 days. (A) Spider plots indicate tumor volumes. Survival panel shows percent surviving mice vs time. (B–G) Foxp3, CD8a/CD8b and Granzyme messenger RNA expression in tumors and spleens from terminal samples. (H) Model of ASO targeting of FOXP3 expression to reduce Treg immunosuppressive capacity and promote antitumor immunity. Data in figure represent two independent experiments. CR, complete responses. Error bars are \pm SEM. *, $p \leq 0.05$; **, $p \leq 0.01$; ***, $p \leq 0.001$; ****, $p \leq 0.0001$ by one-way analysis of variance with Dunnett's post-test relative to PBS group. Survival analysis (A) was done by log-rank Mantel-Cox test. ASOs, antisense oligonucleotides; BIW, two times per week; IFN, interferon; PBS, phosphate buffered saline; PD-1, programmed cell death 1.

as CD25, CTLA-4, CCR4, OX40, ICOS or GITR, but proof of concept has not been established for a specific Treg-targeting agent.⁴³ One major hurdle for these agents is the precision with which Treg depletion can

be demonstrably achieved versus off-target depletion.⁴³ FOXP3 ASOs have the potential to be more selective vs other immune cell types, and thus may offer significant advantages over other Treg-targeting mechanisms

and modalities. Antibody-dependent cellular cytotoxicity (ADCC)-dependent Treg depleting antibodies such as α CTLA4 or α CD25 have shown preclinical efficacy in tumor models,^{44 45} but they also deplete subsets of activated effector cells which express CTLA4 and/or CD25.^{11 46} Moreover, depletion relies on cellular clearance by cell populations bearing relevant Fc receptors, which broadly encompass myeloid and/or natural killer (NK) cells.⁴⁷ Therefore, the utility of Treg depleting antibodies is limited to TMEs harboring both regulatory T-cell and Fc receptor-bearing innate cells. Furthermore, the clinical utility of such approaches could be limited by toxicities related to non-Treg targeting.⁴⁸ While additional antibody targets beyond CTLA4 have been proposed to exhibit a mechanism of action based on Treg depletion,⁴⁹ to our knowledge these molecules have not progressed beyond early clinical proof-of-concept studies in cancer. GITR and OX40 agonist antibodies tested in Ph1 clinical trials depleted tumor Tregs, however, these antibodies only target a subpopulation of tumor Tregs.⁵⁰ Interestingly, apoptotic Tregs can generate a highly immunosuppressive microenvironment by releasing ATP which is then converted to immunosuppressive adenosine,⁵¹ highlighting another caveat of a Treg cell depletion approach. An alternative approach involves targeting Tregs with small molecules, of which several Treg-targeting approaches have been proposed but remain to be tested clinically.⁵² Deconvoluting Treg-dependent versus independent effects remains a challenge for many of these targets. There is a potential utility of PI3K δ small molecule inhibitors to selectively reduce intratumoral Treg frequencies in solid tumors,⁵³ however more recent studies have identified additional direct effects of PI3K δ inhibition on non-Treg populations.⁵⁴ Recently, new drugs targeting the IL-2 pathway have entered clinical trials aiming to deplete Tregs more selectively⁵⁵ and results from these studies will be key to address whether selectively targeting Tregs either by depletion or reprogramming benefits patients.

Several developmental challenges and biological uncertainties remain around Treg biology. Mice do not faithfully model the toxicities observed with immune-based cancer therapeutics in the clinic, and any clinical application would necessitate a careful evaluation of the therapeutic index. Moreover, while highly activated Tregs have been described in clinical biopsies,^{7 56} and overall Tregs have been associated with negative patient outcomes across multiple indications, the presence of Tregs has also been linked to positive patient outcomes in some settings.⁵⁷ FOXP3⁺ Tregs were associated with improved survival in colorectal, head and neck, and esophageal cancers.^{4 5} In colorectal cancers, functionally distinct subpopulations of tumor-infiltrating FOXP3⁺ T cells contribute in opposing ways to determine CRC prognosis and FOXP3 low fraction with a proinflammatory profile showing better overall survival than FOXP3 high.⁵⁸ Thus, a careful evaluation of clinical opportunities is required to enhance the success of this approach. Nonetheless,

provided that a Treg-targeted therapeutic could indeed be safely administered, several exciting clinical opportunities could be explored. Our preclinical data suggest that Treg-targeted therapeutics may be relevant in both monotherapeutic and combination settings (figures 5–7). Several cancers have been characterized by high Treg infiltration,⁴ including melanoma, non-small-cell lung, gastric and ovarian cancers⁴³ and potentially could respond to FOXP3 ASO monotherapy. FOXP3⁺ Tregs have also been linked to a lack of response and resistance to PD-1/PD-L1 checkpoint inhibition,^{40 41 59} and contribution to hyperprogression⁶⁰ which suggest opportunities for benefit from combination therapy.

Our findings support the use of FOXP3 ASOs as a selective therapeutic approach to target tumor Tregs. Importantly, long-term dosing with FOXP3 ASO showed no signs of overt autoimmunity in immuno-competent mice with quick recovery of FOXP3 knockdown and immune activation. In the assay conditions tested, and preclinical models investigated, we have not observed a switch to either a Th1 or Th17 repolarization of Tregs that lost FOXP3, but alternative model systems such as lineage-tracing mouse models could be explored in the future for a more precise evaluation. We have shown that reducing FOXP3 levels led to reduced iTreg suppressive activity *ex vivo*, and importantly promoted a reduction of immunosuppressive markers on Tregs and enhanced T cell activation phenotype in tumor models *in vivo*. There are certain limitations of the iTreg model for example, differences in epigenetic marks, gene expression and stability of immunosuppressive phenotype of iTregs relative to tumor-infiltrating Tregs.^{61 62} It still remains to be formally demonstrated whether ASO-driven reduction of FOXP3 in tumor Tregs leads to the reduction in their immunosuppressive activity *in vivo* and whether this is the main mechanism of the antitumor responses in our preclinical models. nTregs and iTregs have specific and overlapping functions in immunosuppressive responses.⁶¹ In preliminary work we observed high donor variability in suppressive function of human nTregs isolated from PBMCs with the FOXP3 ASO (data not shown) which did not allow us to conclude reduced suppression. This may be due to differences in Treg subsets such as epigenetic make-up⁶² or due to these cells being less homogenous than iTregs. Importantly, we showed targeting tumor FOXP3⁺ Tregs in preclinical tumor models led to antitumor responses. Future studies will be needed to address the exact effects of reducing FOXP3 levels in nTregs and iTregs on T cell function as well as the fate of FOXP3-depleted Tregs.^{63–65}

A small subpopulation of human CD4⁺ and CD8⁺ T cells was shown to transiently up-regulate FOXP3 on *in vitro* stimulation for example, T cell receptor (TCR) stimulation.²⁷ Although their functional role is yet to be fully defined, there is no evidence that they become immunosuppressive or suppress Th1 polarization but seem to have a role in limiting antitumor efficacy.^{27 66–68} We have shown that AZD8701 can suppress FOXP3 expression in all T cell subsets aligned with extensive characterization

of ASO uptake and activity in human T cells and in preclinical models.⁶⁹

Finally, these findings highlight the opportunity to selectively modulate the Treg immuno-suppressive program through inhibition of the previously undruggable transcription factor FOXP3 with AZD8701 and will allow clinical testing of therapeutic hypotheses in patients with cancer with tumors having high Treg infiltration. The combination of FOXP3 inhibition in conjunction with checkpoint blockade has the exciting potential to both broaden and further enhance the clinical impact of these established immuno-oncology therapeutics. Clinical studies with AZD8701 are currently ongoing in patients with advanced solid tumors (NCT04504669).

Author affiliations

¹Ionis Pharmaceuticals, Carlsbad, California, USA

²Oncology R&D, AstraZeneca, Cambridge, UK

³Clinical Pharmacology and Safety Sciences, R&D, AstraZeneca, Cambridge, UK

⁴Oncology R&D, AstraZeneca, Waltham, MA, USA

Acknowledgements The authors would like to thank Tracy Reigle and Raul Alonzo for assistance with figures and manuscript preparation. Schematic figure created using Biorender.com.

Contributors Conceptualization: AR, LSC, CS, FWG, ARM. Flow and mass cytometry analysis: AR, CS, JW, AMH, LSC, LM, MS, GK, MK. Performed in vitro assays: AR, CS, BJ, AS, DG, AW, LI, DAM. Performed in vivo studies: BJ, LH, AP, MT, MM, MC. Transcriptional analysis: BJ, LH, MAT. IHC and histopathology: MC, SK, VS. Writing manuscript: AR, LSC, CS, FWG, ARM. Resources and conceptual: STB, PL, ME, SF. Guarantors: AR, LSC, CS, FWG, ARM. Manuscript review and approval: All authors.

Funding AstraZeneca has a governance framework and processes in place to ensure that commercial sources have appropriate patient consent and ethical approval in place for collection of the samples for research purposes including use by for-profit companies. This report is an independent research, NHS Blood & Transplant have provided material in support of the research. The views expressed in this publication are those of the author(s) and not necessarily those of NHS Blood & Transplant. The AstraZeneca Biobank in the UK is licensed by the Human Tissue Authority (License No. 12109) and has National Research Ethics Service Committee (NREC) Approval as a Research Tissue Bank (RTB) (REC No 17/NW/0207) which covers the use of the samples for this project.

Competing interests The authors are paid employees of AstraZeneca or Ionis Pharmaceuticals, as indicated by their affiliations.

Patient consent for publication Not applicable.

Ethics approval Not applicable.

Provenance and peer review Not commissioned; externally peer reviewed.

Data availability statement Data are available upon reasonable request.

Supplemental material This content has been supplied by the author(s). It has not been vetted by BMJ Publishing Group Limited (BMJ) and may not have been peer-reviewed. Any opinions or recommendations discussed are solely those of the author(s) and are not endorsed by BMJ. BMJ disclaims all liability and responsibility arising from any reliance placed on the content. Where the content includes any translated material, BMJ does not warrant the accuracy and reliability of the translations (including but not limited to local regulations, clinical guidelines, terminology, drug names and drug dosages), and is not responsible for any error and/or omissions arising from translation and adaptation or otherwise.

Open access This is an open access article distributed in accordance with the Creative Commons Attribution Non Commercial (CC BY-NC 4.0) license, which permits others to distribute, remix, adapt, build upon this work non-commercially, and license their derivative works on different terms, provided the original work is properly cited, appropriate credit is given, any changes made indicated, and the use is non-commercial. See <http://creativecommons.org/licenses/by-nc/4.0/>.

ORCID iDs

Alexey Revenko <http://orcid.org/0000-0002-4863-362X>

Larissa S Carnevali <http://orcid.org/0000-0001-7432-0195>

Adina M Hughes <http://orcid.org/0000-0002-5711-627X>

Deanna A Mele <http://orcid.org/0000-0002-6429-4269>

Frederick W Goldberg <http://orcid.org/0000-0002-4874-1700>

REFERENCES

- Sakaguchi S, Yamaguchi T, Nomura T, et al. Regulatory T cells and immune tolerance. *Cell* 2008;133:775–87.
- Josefowicz SZ, Lu L-F, Rudensky AY. Regulatory T cells: mechanisms of differentiation and function. *Annu Rev Immunol* 2012;30:531–64.
- Whiteside TL. What are regulatory T cells (Treg) regulating in cancer and why? *Semin Cancer Biol* 2012;22:327–34.
- Shang B, Liu Y, Jiang S-juan, et al. Prognostic value of tumor-infiltrating FoxP3+ regulatory T cells in cancers: a systematic review and meta-analysis. *Sci Rep* 2015;5:15179.
- Salama P, Phillips M, Griev F, et al. Tumor-infiltrating FOXP3+ T regulatory cells show strong prognostic significance in colorectal cancer. *J Clin Oncol* 2009;27:186–92.
- Preston CC, Maurer MJ, Oberg AL, et al. The ratios of CD8+ T cells to CD4+CD25+ FOXP3+ and FOXP3- T cells correlate with poor clinical outcome in human serous ovarian cancer. *PLoS One* 2013;8:e80063.
- Plitas G, Konopacki C, Wu K, et al. Regulatory T cells exhibit distinct features in human breast cancer. *Immunity* 2016;45:1122–34.
- Beyer M, Schultze JL. Regulatory T cells in cancer. *Blood* 2006;108:804–11.
- Shitara K, Nishikawa H. Regulatory T cells: a potential target in cancer immunotherapy. *Ann N Y Acad Sci* 2018;1417:104–15.
- Owen DL, Mahmud SA, Sjaastad LE, et al. Thymic regulatory T cells arise via two distinct developmental programs. *Nat Immunol* 2019;20:195–205.
- Sharma A, Subudhi SK, Blando J, et al. Anti-CTLA-4 Immunotherapy Does Not Deplete FOXP3+ Regulatory T Cells (Tregs) in Human Cancers-Response. *Clin Cancer Res* 2019;25:3469–70.
- Hori S, Nomura T, Sakaguchi S. Control of regulatory T cell development by the transcription factor Foxp3. *Science* 2003;299:1057–61.
- Fontenot JD, Gavin MA, Rudensky AY. Foxp3 programs the development and function of CD4+CD25+ regulatory T cells. *Nat Immunol* 2003;4:330–6.
- Bennett CL, Christie J, Ramsdell F, et al. The immune dysregulation, polyendocrinopathy, enteropathy, X-linked syndrome (IPEX) is caused by mutations of FOXP3. *Nat Genet* 2001;27:20–1.
- Klages K, Mayer CT, Lahl K, et al. Selective depletion of Foxp3+ regulatory T cells improves effective therapeutic vaccination against established melanoma. *Cancer Res* 2010;70:7788–99.
- Bos PD, Plitas G, Rudra D, et al. Transient regulatory T cell ablation deters oncogene-driven breast cancer and enhances radiotherapy. *J Exp Med* 2013;210:2435–66.
- Crooke ST, Witztum JL, Bennett CF, et al. RNA-Targeted therapeutics. *Cell Metab* 2018;27:714–39.
- Bennett CF, Baker BF, Pham N, et al. Pharmacology of antisense drugs. *Annu Rev Pharmacol Toxicol* 2017;57:81–105.
- Crooke ST. Molecular mechanisms of antisense oligonucleotides. *Nucleic Acid Ther* 2017;27:70–7.
- Seth PP, Siwkowski A, Allerson CR, et al. Short antisense oligonucleotides with novel 2'-4' conformationally restricted nucleoside analogues show improved potency without increased toxicity in animals. *J Med Chem* 2009;52:10–13.
- Murray S, Ittig D, Koller E, et al. TricycloDNA-modified oligo-2'-deoxyribonucleotides reduce scavenger receptor B1 mRNA in hepatic and extra-hepatic tissues—a comparative study of oligonucleotide length, design and chemistry. *Nucleic Acids Res* 2012;40:6135–43.
- Hong D, Kurzrock R, Kim Y, et al. AZD9150, a next-generation antisense oligonucleotide inhibitor of STAT3 with early evidence of clinical activity in lymphoma and lung cancer. *Sci Transl Med* 2015;7:ra185.
- Reilly MJ, McCoon P, Cook C, et al. STAT3 antisense oligonucleotide AZD9150 in a subset of patients with heavily pretreated lymphoma: results of a phase 1b trial. *J Immunother Cancer* 2018;6:119.
- Chowdhury S, Burris HA, Patel M, et al. A phase I dose escalation, safety and pharmacokinetic (PK) study of AZD5312 (IONIS-ARRx), a first-in-class generation 2.5 antisense oligonucleotide targeting the androgen receptor (AR). *Eur J Cancer* 2016;69:S145.
- Allan SE, Crome SQ, Crellin NK, et al. Activation-induced FOXP3 in human T effector cells does not suppress proliferation or cytokine production. *Int Immunol* 2007;19:345–54.

- 26 Wang J, Ioan-Facsinay A, van der Voort EI, *et al.* Transient expression of FOXP3 in human activated nonregulatory CD4⁺ T cells. *Eur J Immunol* 2007;37:129–38.
- 27 Lozano T, Conde E, Martín-Otal C, *et al.* TCR-induced FOXP3 expression by CD8⁺ T cells impairs their anti-tumor activity. *Cancer Lett* 2022;528:45–58.
- 28 Curotto de Lafaille MA, Lafaille JJ, Lafaille Cde. Natural and adaptive foxp3⁺ regulatory T cells: more of the same or a division of labor? *Immunity* 2009;30:626–35.
- 29 Webster KE, Walters S, Kohler RE, *et al.* In vivo expansion of T reg cells with IL-2-mAb complexes: induction of resistance to EAE and long-term acceptance of islet allografts without immunosuppression. *J Exp Med* 2009;206:751–60.
- 30 Marson A, Kretschmer K, Frampton GM, *et al.* Foxp3 occupancy and regulation of key target genes during T-cell stimulation. *Nature* 2007;445:931–5.
- 31 Zheng L, Sharma R, Gaskin F, *et al.* A novel role of IL-2 in organ-specific autoimmune inflammation beyond regulatory T cell checkpoint: both IL-2 knockout and Fas mutation prolong lifespan of Scurfy mice but by different mechanisms. *J Immunol* 2007;179:8035–41.
- 32 Gavin MA, Rasmussen JP, Fontenot JD, *et al.* Foxp3-dependent programme of regulatory T-cell differentiation. *Nature* 2007;445:771–5.
- 33 Kwon H-K, Chen H-M, Mathis D, *et al.* FoxP3 scanning mutagenesis reveals functional variegation and mild mutations with atypical autoimmune phenotypes. *Proc Natl Acad Sci U S A* 2018;115:E253–62.
- 34 Williams LM, Rudensky AY. Maintenance of the Foxp3-dependent developmental program in mature regulatory T cells requires continued expression of Foxp3. *Nat Immunol* 2007;8:277–84.
- 35 Mayer CT, Ghorbani P, Köhl AA, *et al.* Few Foxp3⁺ regulatory T cells are sufficient to protect adult mice from lethal autoimmunity. *Eur J Immunol* 2014;44:2990–3002.
- 36 Barzaghi F, Passerini L, Gambineri E, *et al.* Demethylation analysis of the FOXP3 locus shows quantitative defects of regulatory T cells in IPEX-like syndrome. *J Autoimmun* 2012;38:49–58.
- 37 Elkord E, Al-Ramadi BK. Helios expression in FoxP3(+) T regulatory cells. *Expert Opin Biol Ther* 2012;12:1423–5.
- 38 Mosely SIS, Prime JE, Sainson RCA, *et al.* Rational selection of syngeneic preclinical tumor models for immunotherapeutic drug discovery. *Cancer Immunol Res* 2017;5:29–41.
- 39 Taylor MA, Hughes AM, Walton J, *et al.* Longitudinal immune characterization of syngeneic tumor models to enable model selection for immune oncology drug discovery. *J Immunother Cancer* 2019;7:328.
- 40 Dodagatta-Marri E, Meyer DS, Reeves MQ, *et al.* α -PD-1 therapy elevates Treg/Th balance and increases tumor cell pSmad3 that are both targeted by α -TGF β antibody to promote durable rejection and immunity in squamous cell carcinomas. *J Immunother Cancer* 2019;7:62.
- 41 Kumagai S, Togashi Y, Kamada T, *et al.* The PD-1 expression balance between effector and regulatory T cells predicts the clinical efficacy of PD-1 blockade therapies. *Nat Immunol* 2020;21:1346–58.
- 42 Finan C, Gaulton A, Kruger FA, *et al.* The druggable genome and support for target identification and validation in drug development. *Sci Transl Med* 2017;9. doi:10.1126/scitranslmed.aag1166. [Epub ahead of print: 29 03 2017].
- 43 Togashi Y, Shitara K, Nishikawa H. Regulatory T cells in cancer immunosuppression - implications for anticancer therapy. *Nat Rev Clin Oncol* 2019;16:356–71.
- 44 Arce Vargas F, Furness AJS, Solomon I, *et al.* Fc-Optimized Anti-CD25 depletes tumor-infiltrating regulatory T cells and synergizes with PD-1 blockade to eradicate established tumors. *Immunity* 2017;46:577–86.
- 45 Selby MJ, Engelhardt JJ, Quigley M, *et al.* Anti-CTLA-4 antibodies of IgG2a isotype enhance antitumor activity through reduction of intratumoral regulatory T cells. *Cancer Immunol Res* 2013;1:32–42.
- 46 Quezada SA, Peggs KS. Lost in translation: deciphering the mechanism of action of anti-human CTLA-4. *Clin Cancer Res* 2019;25:1130–2.
- 47 Nimmerjahn F, Ravetch JV. Fc γ receptors as regulators of immune responses. *Nat Rev Immunol* 2008;8:34–47.
- 48 Di Giacomo AM, Biagioli M, Maio M. The emerging toxicity profiles of anti-CTLA-4 antibodies across clinical indications. *Semin Oncol* 2010;37:499–507.
- 49 Klebanoff CA, Gattinoni L. Stubborn Tregs limit T-cell therapy. *Blood* 2012;120:2352–4.
- 50 Zappasodi R, Sirard C, Li Y, *et al.* Rational design of anti-GITR-based combination immunotherapy. *Nat Med* 2019;25:759–66.
- 51 Maj T, Wang W, Crespo J, *et al.* Oxidative stress controls regulatory T cell apoptosis and suppressor activity and PD-L1-blockade resistance in tumor. *Nat Immunol* 2017;18:1332–41.
- 52 Crooke ST, Wang S, Vickers TA, *et al.* Cellular uptake and trafficking of antisense oligonucleotides. *Nat Biotechnol* 2017;35:230–7.
- 53 Ali K, Soond DR, Pineiro R, *et al.* Inactivation of PI(3)K p110 δ breaks regulatory T-cell-mediated immune tolerance to cancer. *Nature* 2014;510:407–11.
- 54 Carnevalli LS, Sinclair C, Taylor MA, *et al.* PI3K α/δ inhibition promotes anti-tumor immunity through direct enhancement of effector CD8⁺ T-cell activity. *J Immunother Cancer* 2018;6:158.
- 55 Solomon I, Amann M, Goubier A, *et al.* CD25-T_{reg}-depleting antibodies preserving IL-2 signaling on effector T cells enhance effector activation and antitumor immunity. *Nat Cancer* 2020;1:1153–66.
- 56 De Simone M, Arrigoni A, Rossetti G, *et al.* Transcriptional landscape of human tissue lymphocytes unveils uniqueness of tumor-infiltrating T regulatory cells. *Immunity* 2016;45:1135–47.
- 57 Lukesova E, Boucek J, Rotnaglova E, *et al.* High level of Tregs is a positive prognostic marker in patients with HPV-positive oral and oropharyngeal squamous cell carcinomas. *Biomed Res Int* 2014;2014:1–11.
- 58 Saito T, Nishikawa H, Wada H, *et al.* Two FOXP3(+)CD4(+) T cell subpopulations distinctly control the prognosis of colorectal cancers. *Nat Med* 2016;22:679–84.
- 59 Huang AC, Orlowski RJ, Xu X, *et al.* A single dose of neoadjuvant PD-1 blockade predicts clinical outcomes in resectable melanoma. *Nat Med* 2019;25:454–61.
- 60 Kim CG, Kim KH, Pyo K-H, *et al.* Hyperprogressive disease during PD-1/PD-L1 blockade in patients with non-small-cell lung cancer. *Ann Oncol* 2019;30:1104–13.
- 61 Wei T, Zhong W, Li Q. Role of heterogeneous regulatory T cells in the tumor microenvironment. *Pharmacol Res* 2020;153:104659.
- 62 Miyao T, Floess S, Setoguchi R, *et al.* Plasticity of Foxp3(+) T cells reflects promiscuous Foxp3 expression in conventional T cells but not reprogramming of regulatory T cells. *Immunity* 2012;36:262–75.
- 63 Overacre-Delgoffe AE, Chikina M, Dadey RE, *et al.* Interferon- γ Drives T_{reg} Fragility to Promote Anti-tumor Immunity. *Cell* 2017;169:1130–41.
- 64 Chaudhry A, Rudra D, Treuting P, *et al.* CD4⁺ regulatory T cells control TH17 responses in a Stat3-dependent manner. *Science* 2009;326:986–91.
- 65 Levine AG, Mendoza A, Hemmers S, *et al.* Stability and function of regulatory T cells expressing the transcription factor T-bet. *Nature* 2017;546:421–5.
- 66 Ahmadzadeh M, Antony PA, Rosenberg SA. IL-2 and IL-15 each mediate de novo induction of FOXP3 expression in human tumor antigen-specific CD8 T cells. *J Immunother* 2007;30:294–302.
- 67 Gavin MA, Torgerson TR, Houston E, *et al.* Single-cell analysis of normal and FOXP3-mutant human T cells: FOXP3 expression without regulatory T cell development. *Proc Natl Acad Sci U S A* 2006;103:6659–64.
- 68 Tran DQ, Ramsey H, Shevach EM. Induction of FOXP3 expression in naive human CD4⁺FOXP3 T cells by T-cell receptor stimulation is transforming growth factor-beta dependent but does not confer a regulatory phenotype. *Blood* 2007;110:2983–90.
- 69 Proia TA, Singh M, Woessner R, *et al.* STAT3 Antisense Oligonucleotide Remodels the Suppressive Tumor Microenvironment to Enhance Immune Activation in Combination with Anti-PD-L1. *Clin Cancer Res* 2020;26:6335–49.

Supplemental materials.

Supplemental Materials and Methods.

In vivo expansion of Tregs

Tregs were expanded *in vivo* with IL-2–anti-IL-2 mAb (JES6-1) complexes as previously described¹. Recombinant mouse IL-2 (Biolegend) was mixed with anti-IL-2 mAb (clone JES6-1A12, Biolegend) at a 2:1 molar ratio and incubated at 37°C for 30 min. Mice were intraperitoneally injected with 6 µg of complexes (1 µg of IL-2 and 5 µg of anti-IL-2 antibody) for 3 consecutive days. Spleens were harvested 24 hours after the last injection (at this timepoint Tregs were expanded 3-4-fold) and splenocytes were isolated by mechanical disruption of spleens in tissue dissociation tubes (Miltenyi) on gentleMACS dissociator (Miltenyi). CD4 T cells were isolated from splenocytes using mouse Easysep CD4 T cell purification kit (Stemcell Technologies). Purified CD4 cells were cultured in TexMACS media (Miltenyi) supplemented with 30 ng/mL of mouse recombinant IL-2 (Biolegend). CD4 cells were treated *ex-vivo* with oligonucleotides by free uptake in a dose-response study for 72 hours and collected for RNA extraction and RT-qPCR analysis.

Vaccination study

Mice were vaccinated with 10 µg ovalbumin + adjuvant (AddaVax™) in 50 µL injection volume via IM injection on the alternating left and right quadriceps sites on Days 15 and 37. ASOs were administered via SC injection in alternating areas of the dorsal region at 40 mg/kg/dose on 5 days on and 2 days off regimen. On day 43 animals were sacrificed and blood was collected into EDTA anticoagulant for hematological analysis and an aliquot stored at -80°C for analysis of immune endpoints.

Cell culture and reagents

Human SUP-M2 anaplastic large cell lymphoma cells (ATCC) were cultured in RPMI-1640 media supplemented with 10% FBS (Thermo Fisher Scientific). Cells were incubated in media containing different concentrations of FOXP3 or control ASOs and harvested 48-72 hours later for human *FOXP3* mRNA RT-qPCR analysis.

Murine primary immune cells were derived from spleens. Human PBMCs were purchased from allcells.com or derived from leukocyte cones (NHS Blood and Transplant Service (NHSBT, UK) and Stemcell Technologies) as anonymized samples from consenting donors.

Cell cultures were performed in complete RPMI (RPMI supplemented with 10% FCS, non-essential amino acids (Thermo Fisher Scientific, 1X concentration), Sodium pyruvate (1 mM), glutamine (4 mM), penicillin and streptomycin (Sigma Aldrich, 1X), 2-mercaptoethanol (50 μ M) and HEPES (2 mM)), in TexMACS media (Miltenyi) or in ImmunoCult™-XF T Cell Expansion Medium (Stemcell Technologies).

Recombinant human IL-2 and murine IL-2 were purchased from Peprotech, Stemcell Technologies and Biolegend, and recombinant human TGF β was purchased from R&D Systems. α mouse IL-2 neutralizing antibody (clone JES6-1A12) was purchased from Biolegend.

RNA extraction and analysis

Cultured adherent cells or pelleted suspension cells were directly lysed in RLT buffer (QIAGEN) containing 1% 2-mercaptoethanol. Tissues from mice (spleens, tumors etc) were homogenized in RLT buffer (QIAGEN) containing 1% 2-mercaptoethanol. Total mRNA was prepared using PureLink™ Pro 96 RNA total RNA isolation kit (Invitrogen, Life Technologies, Carlsbad, CA) according to the manufacturer's instructions. The amount of

specific mRNA was analyzed using a StepOne™ Real-Time PCR System (Applied Biosystems, Life Technologies, Carlsbad, CA). Target gene RNA expression was normalized to the total RNA levels measured by RiboGreen (Invitrogen, Life Technologies, Carlsbad, CA) or to the RNA levels of the housekeeping gene, GAPDH. The sequences of primer-probe sets (PPS) for RT-qPCR analysis are listed in Table 1.

Fluidigm gene expression analysis was performed as described previously ².

Treg isolation and in vitro culture

Murine and human Tregs and CD4⁺ cells were isolated using EasySep™ Mouse CD4+CD25⁺ Regulatory T cell isolation kit II, and EasySep™ Human CD4+CD127^{low}CD25⁺ regulatory T-cell kits respectively (Stemcell Technologies), according to the manufacturer's instructions.

Inducible Tregs were generated by activating CD4⁺ T-cell precursors with Dynabeads Human T-Activator CD3/CD28 beads or Dynabeads Mouse T-Activator CD3/CD28 beads (Thermofisher), in the additional presence of 10 ng/mL species matched IL-2 and 20 ng/mL human TGFβ for 4-5 days. iTregs were differentiated in the presence of 5 μM (mouse) or 1 μM (human) ASO.

Primary Tregs were cultured in cRPMI with 10 ng/mL mIL-2 (mouse) or 5 ng/mL hIL-2 (human), in the additional presence of ASOs as indicated. Human Tregs were additionally activated with Dynabeads Human T-Activator CD3/CD28 beads (Thermofisher) for the final two days of culture.

Treg in vitro suppression assays

For mouse assays, CD4⁺ T-cells were labeled with CTV as previously described³, and 2.5×10^4 activated with soluble α CD3 (clone 17A2, BD) in and 5×10^5 murine B-cells that were isolated from spleens of WT mice with an EasySep™ Mouse B Cell Isolation Kit, in 96-well round-bottom plates. iTregs were added to cultures at differing ratios, along with 5 μ M ASO. After 3 days, cell proliferation was profiled by flow cytometry.

For human assays, CTV labeled CD4⁺ T-cells (5×10^4) were activated with Dynabeads Human T-Activator CD3/CD28 beads (6.25×10^3), in the presence of varying ratios of autologous iTregs. Cultures were performed in 96-well round-bottom plates in the presence of 1 μ M ASO and analyzed by flow cytometry after 3 days.

Flow cytometry

The following fluorophore-conjugated antibodies were used in this study: α -mouse CD47 (clone miap301), α -mouse CD45 (30-F11), α -mouse (53-6.7) CD4 (RM4-5), α -mouse PD-1 (29F.1.A12), α -mouse Granzyme B (GB12), α -mouse CD25 (BC96), α -mouse Foxp3 (FJK-16S and 150D), α -mouse CD3 ϵ (17A2) α -mouse CD69 (H1.2F3), α -mouse CD62L (MEL14), α -mouse/human CD44 (IM7), α -mouse CTLA4 (UC10-4B9), α -mouse GITR (DTA-1), α -mouse CD73 (eBioTY.11.8), α -mouse CD19 (ID3), α -mouse/human Helios (22F6), α -human CTLA4 (L3D10), α -ICOS (C398.4A), α -human CCR8 (L26368), α -human GITR (eBioAITR), α -human CD3 (SK7 and UHCT1), α -human CD25 (BC96), α -human CD4 (OKT4), α -human CD8 (RPA.T8 and SK1), α -human CD45 (2D1).

All antibodies were purchased from Biolegend, Thermo-Fisher Scientific or BD Biosciences. Cells were stained with a viability marker (Live/Dead Aqua® from Thermo-Fisher Scientific or Zombie-NIR from Biolegend) according to manufacturer's instructions and stained for

surface/intracellular markers in the presence of saturating concentrations of CD16/32 FC-blocking antibodies as described previously ⁴.

Samples were filtered through 40 µm cell strainers, acquired on a BD LSRFortessa or Attune NxT cytometer, and downstream analysis was performed using FlowJo software (V10) or Attune NxT Software (V2.5).

Mass Cytometry

Tumor tissues were chopped and transferred into a tube containing RPMI (Thermo Fisher, Gibco 61870-044). Single-cell suspension was prepared by treating tumors with mouse tumor dissociation kit (Miltenyi Biotec; No. 130-096-730) for 40 minutes at 37°C with agitation. 3×10^6 cells per sample were stained with 5 µmol/L Cell-ID Cisplatin (Fluidigm, No. 201064), divided into pools of 20 samples and barcoded using the Cell-ID 20-Plex Pd Barcoding Kit (Fluidigm; No. 201060) according to the manufacturer's instructions. Cells were blocked with anti-CD16/CD32 antibody (Thermo Fisher; 14-0161-86) and stained overnight with metal- or fluorophore-conjugated antibodies (Supplementary Table S5) in Perm Buffer (Thermo Fisher; 00-8333-56). Antibodies (Supplementary Table 1) that were not available as metal conjugates were labeled using Maxpar X8 Antibody Labeling Kits (Fluidigm; 201141A–201156A and 201158A–201176A; Sigma, No. 203440) according to the manufacturer's instructions or as published elsewhere ⁵. Samples were washed twice and stained using metal-conjugated secondary antibodies incubated for 30 minutes at 4°C, washed twice, and stored in MaxPar Fix and Perm Buffer (Fluidigm; No. 201067) with Cell-ID Intercalator-Ir (Fluidigm; 201192A) at 125 nmol/L until acquisition. Compensation of spectral overlap between antibodies was performed using beads (BD Biosciences; No. 552843 and No. 552845) stained with each of the metal-conjugated antibodies. Stained beads were then pooled for acquisition.

Immediately before acquisition, beads or tumor samples were washed twice using Cell Staining Buffer (Fluidigm; No. 201068) and then twice with MaxPar Cell Acquisition Solution (Fluidigm; No. 201240). Pellets were filtered twice through 70- μ m strainer (Greiner No. 542070) and acquired on Helios CyTOF System (Fluidigm). Sample de-barcoding was performed using CyTOF Software (Fluidigm) or manual gating, and data were analyzed using FlowJo software (V.10, Treestar) or Cytobank. Data compensation was performed using CATALYST package (20).

CyTOF data analysis

Cell clustering was performed with [FlowSOM](#)⁶ and [ConsensusClusterPlus](#)⁷ using ‘cluster’ function in CATALYST package (ref). The identified clusters (n=10) were visualized using tSNE based on cytofWorkflow (<https://github.com/markrobinsonuzh/cytofWorkflow>). Statistical significance of differences of median marker intensities (arcsinh-transformed) across conditions were evaluated using two-sided t-test and p-values were adjusted using Benjamini Hochberg method.

Immunohistochemistry

Mouse FOXP3 protein was detected in FFPE fixed tumors using FoxP3 (FJK-16s) eBioscience™/ThermoFisher Validation IHC at a 1:50 dilution. In brief, after removal, tumors were fixed in 10% neutral-buffered formalin (NBF) and embedded in paraffin wax. 4-micrometer thick sections were stained on a Ventana Discovery Ultra. Antigen retrieval was done using the CC1 protocol. Vector ABC HRP Kit (PK-6104) was used for chromogenic detection.

ELISA detection of cytokines and IgG

A panel of cytokines comprising IFN γ , TNF α , MCP-1, IL-1 β , IL-2, IL-4, IL-6, IL-10, IL-17a and KC was assessed in EDTA plasma by multiplex bead array assay (MILLIPLEX® MAP mouse Cytokine/Chemokine, Millipore Corporation, Billerica, MA, USA) following manufacturer's instructions. In brief, 25 μ l samples, standards and controls were incubated with antibody-immobilized beads and assay buffer for 17 hours at 4°C on an orbital shaker at 800 rpm. Plates were washed and incubated with 25 μ l detection antibodies for 1h prior to incubation with 25 μ l of Streptavidin-Phycoerythrin for 30 mins. Plates were then washed and 150 μ l of Drive Fluid was added. Fluorescence was measured on Luminex MAGPIX using Luminex xMAP® Technology (Luminex BV, Oosterhout, The Netherlands). All incubations took place on an orbital shaker at 800 rpm at room temperature, unless stated otherwise. The standard curve was generated using 5PL non-linear regression and used to extrapolate cytokine concentrations. Acceptance criteria for controls and standard curve included 20 % CV and % recovery between 80 and 120 %.

To detect OVA-specific IgG, 96 well plates were coated overnight at 4°C with 100 μ L/well 20 mg/mL ovalbumin (Sigma) in PBS. Following blocking with BSA, 50 μ L mouse anti-OVA antibody standards (25 ng/mL to 0.05 ng/mL) or plasma samples were incubated for 1.5 hours at room temperature followed by incubation with 50 μ L HRP conjugated anti-mouse IgG antibody for 1.5 hours at room temperature in the dark. Finally, bound antibody was detected with 100 μ L TMB substrate (Sigma) and the reaction stopped with acid stop solution. Color change was quantified by reading at 450 nm and normalized based on interpolation from a standard curve.

Supplemental references.

1. Webster, K.E. *et al.* In vivo expansion of T reg cells with IL-2-mAb complexes: induction of resistance to EAE and long-term acceptance of islet allografts without immunosuppression. *J Exp Med* **206**, 751-760 (2009).
2. Carnevalli, L.S. *et al.* PI3Kalpha/delta inhibition promotes anti-tumor immunity through direct enhancement of effector CD8(+) T-cell activity. *J Immunother Cancer* **6**, 158 (2018).
3. Langdon, S. *et al.* Combination of dual mTORC1/2 inhibition and immune-checkpoint blockade potentiates anti-tumour immunity. *Oncoimmunology* **7**, e1458810 (2018).
4. Sinclair, C. *et al.* mTOR regulates metabolic adaptation of APCs in the lung and controls the outcome of allergic inflammation. *Science* **357**, 1014-1021 (2017).
5. Han, G., Spitzer, M.H., Bendall, S.C., Fantl, W.J. & Nolan, G.P. Metal-isotope-tagged monoclonal antibodies for high-dimensional mass cytometry. *Nat Protoc* **13**, 2121-2148 (2018).
6. Van Gassen, S. *et al.* FlowSOM: Using self-organizing maps for visualization and interpretation of cytometry data. *Cytometry A* **87**, 636-645 (2015).
7. Wilkerson, M.D. & Hayes, D.N. ConsensusClusterPlus: a class discovery tool with confidence assessments and item tracking. *Bioinformatics* **26**, 1572-1573 (2010).

Supplemental Figure legends.

Supplementary Figure 1. AZD8701 is a potent clinical candidate ASO targeting human FOXP3. (A) FOXP3 mRNA reduction in FOXP3-expressing human SUP-M2 cells by 10 best FOXP3 ASOs *in vitro* was measured by RT-qPCR. N=4 replicates. (B) Primary human Tregs were isolated from human PBMCs and cultured with AZD8701 or control ASO for a total of 9 days in duplicates, in the presence of Dynabeads® human T-activated CD3/CD28 for the final 2 days of culture (see methods). (C) Line graph shows FOXP3 protein abundance in cultured Tregs as measured by flow cytometry. Data represent ≥ 3 independent experiments. (D) NSG mice were humanized were by the infusion of human PBMC and treated systemically with FOXP3 ASOs for 4 consecutive days at 25 mg/kg. FOXP3 mRNA and protein expression was quantified for various FOXP3 ASO candidates by RT-qPCR and flow cytometry. N = 4 per group. (E) Transcript map and sequence of the candidate ASO AZD8701. (F) Human PBMCs were stimulated with anti-CD3/CD28 beads and FOXP3 protein expression measured in CD4 and CD8 T cells by flow cytometry in the presence of CTL ASO or AZD8701 at 1 μ M for 9 days. Error bars are SD (A and B) or SEM (D and F). *, $p \leq 0.05$; **, $p \leq 0.01$; ***, $p \leq 0.001$; ****, $p \leq 0.0001$ by one-way ANOVA with Dunnett's post-test. Differences are calculated relative to PBS.

Supplementary Figure 2. AZD8701 confers dose-dependent pharmacodynamic changes in cultured human primary Tregs. Primary human Tregs were isolated from PBMCs and cultured with indicated concentrations of AZD8701 for 9 days, with Dynabeads® human T-activated CD3/CD28 addition for the final 2 days. (A) Line graphs show the abundance of indicated surface proteins as measured by flow cytometry after treatment with AZD8701. (B)

Pooled samples from donors treated with a range of shortlisted ASOs at varying concentrations were evaluated, to assess the correlation between indicated protein abundance and FOXP3 expression.

Supplementary Figure 3. Human FOXP3 ASOs target FOXP3 signature genes in primary iTregs differentiated for 9 days and activated with CD3/CD28 Dynabeads® for the final 2 days. N=5 replicates. (A) Overview of shared gene signature and immune-related pathways and (B) selected gene expression changes by RNAseq. Error bars are SEM. *, $p \leq 0.05$; **, $p \leq 0.01$; ***, $p \leq 0.001$; ****, $p \leq 0.0001$ by one-way ANOVA with Dunnett's post-test. Differences are calculated relative to control ASO.

Supplementary Figure 4. In vitro activity of mouse Foxp3 ASOs screening in primary mouse Tregs. (A) Primary CD4 cells were isolated from spleens and cultured with mouse Foxp3 or control ASOs for 3 days in duplicates. (B) Quantification IC₅₀ for mouse Foxp3 mRNA for tested ASOs. Error bars are SD.

Supplementary Figure 5. Preliminary safety/tolerability assessments of mouse Foxp3 ASOs in healthy mice. (A) Normal BALB/c mice were treated via s.c. administration, BIW with ASOs for 39 days. N= 5 per group. Line graph shows bodyweight. (B) Representative images of haired skin (10x magnification) and liver (20x magnification) following mouse Foxp3 ASO treatment for 12 weeks. (C) Plasma cytokine profiles following the dosing of mice with two distinct Foxp3 ASOs alongside a control ASO or PBS for 6 and 12 weeks. Data shown represent the mean \pm SD. Data represent 2 independent experiments. (D) Proinflammatory

cytokine and anti-Ova IgG responses following exposure for 6 weeks to ovalbumin and adjuvant alongside with indicated treatments. Data represent the mean \pm SD.

Supplementary Figure 6. Mouse Foxp3 ASOs produce dose-responsive inhibition of FOXP3 expression in Tregs and antitumor effects in the A20 tumor model. A20 tumor-bearing mice were systemically treated with Foxp3 ASOs at indicated doses. N=8 per group. (A) Line graphs show A20 tumor volumes (both individual animal data and group averages). The number of complete responses (CR) vs total number of animals in the group is indicated next to lines. (B) Tumors and spleens were dissociated infiltrating Tregs were analyzed by flow cytometry. Foxp3 protein expression was measured in Helios+ CD4 Tregs. (C) Spleens were dissociated and the frequencies of CD69+ activated T-effector cells and CD62LloCD44hi T-memory cells within the total CD4+ T-cell population were analyzed by flow cytometry. Data represent ≥ 2 independent experiments. Error bars are SEM. *, $p \leq 0.05$; **, $p \leq 0.01$; ***, $p \leq 0.001$; ****, $p \leq 0.0001$ by one-way ANOVA with Dunnett's post-test for B and C and two-way ANOVA with Dunnett's post-test for A. Differences are calculated relative to PBS.

Supplementary Figure 7. A Treg-infiltrated TME typifies mouse Foxp3 ASO-sensitive preclinical models. (A) Representative FOXP3 IHC staining for indicated models. (B) Line graphs show tumor volumes for indicated models and ASOs treatments. N=10 per group. Data represent ≥ 2 independent experiments. Error bars are SEM.

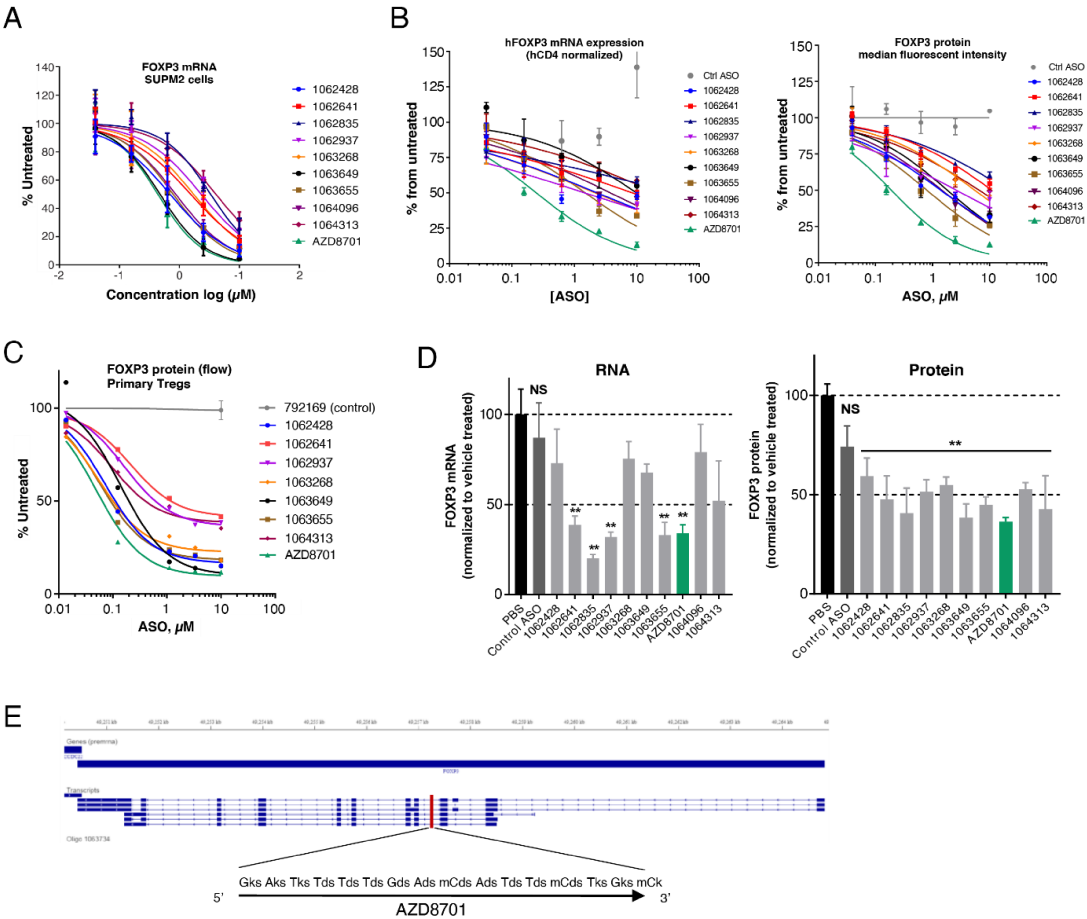
Supplemental Table 1. RT-qPCR primer-probe sets used in this study.

Gene	Forward Primer	Reverse Primer	Probe
Mouse <i>Foxp3</i>	GTACACCCAGGAAA GACAGC	TGCTTGGCAGTGCT TGA	CCAGGCCACTTGC AGACTCCATT
Human <i>FOXP3</i>	CTACTTCAAGTTCC ACAACATGC	CCAGTGGTAGATCT CATTGAGTG	CCTTTCACCTACG CCACGCTCAT
Mouse <i>Gapdh</i>	TGTGTCCGTCGTGG ATCTGA	CCTGCTTCACCACC TTCTTGA	CCGCCTGGAGAA ACCTGCCAAGTAT G
Human <i>GAPDH</i>	GAAGGTGAAGGTCG GAGTC	GAAGGTGAAGGTCG GAGTC	CAAGCTTCCCGTT CTCAGCC

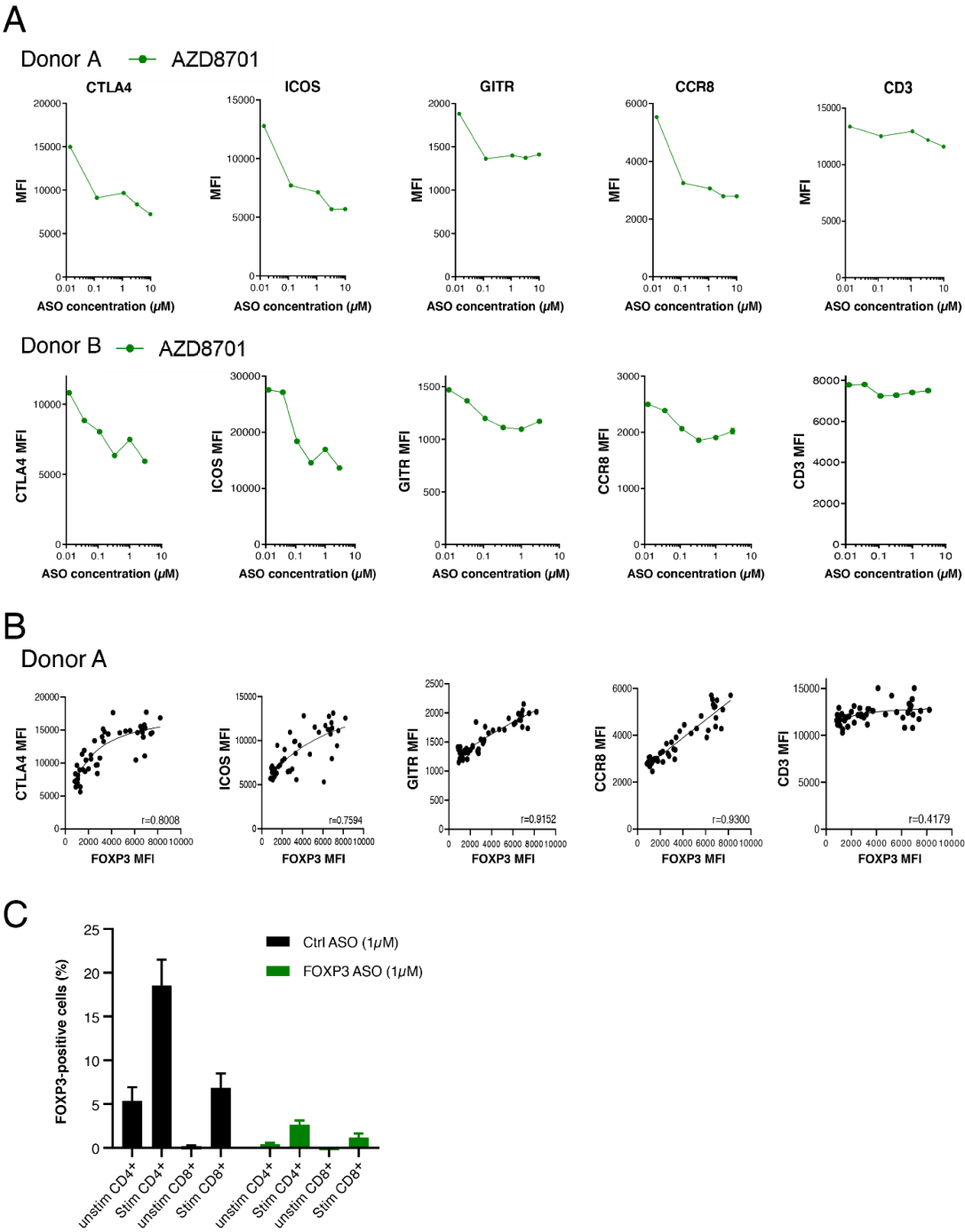
Mouse *Gzmb* (Mm00442837_m1) and mouse *Cd8* (Mm01182107_g1) primer-probe sets

were from ThermoFisher Scientific

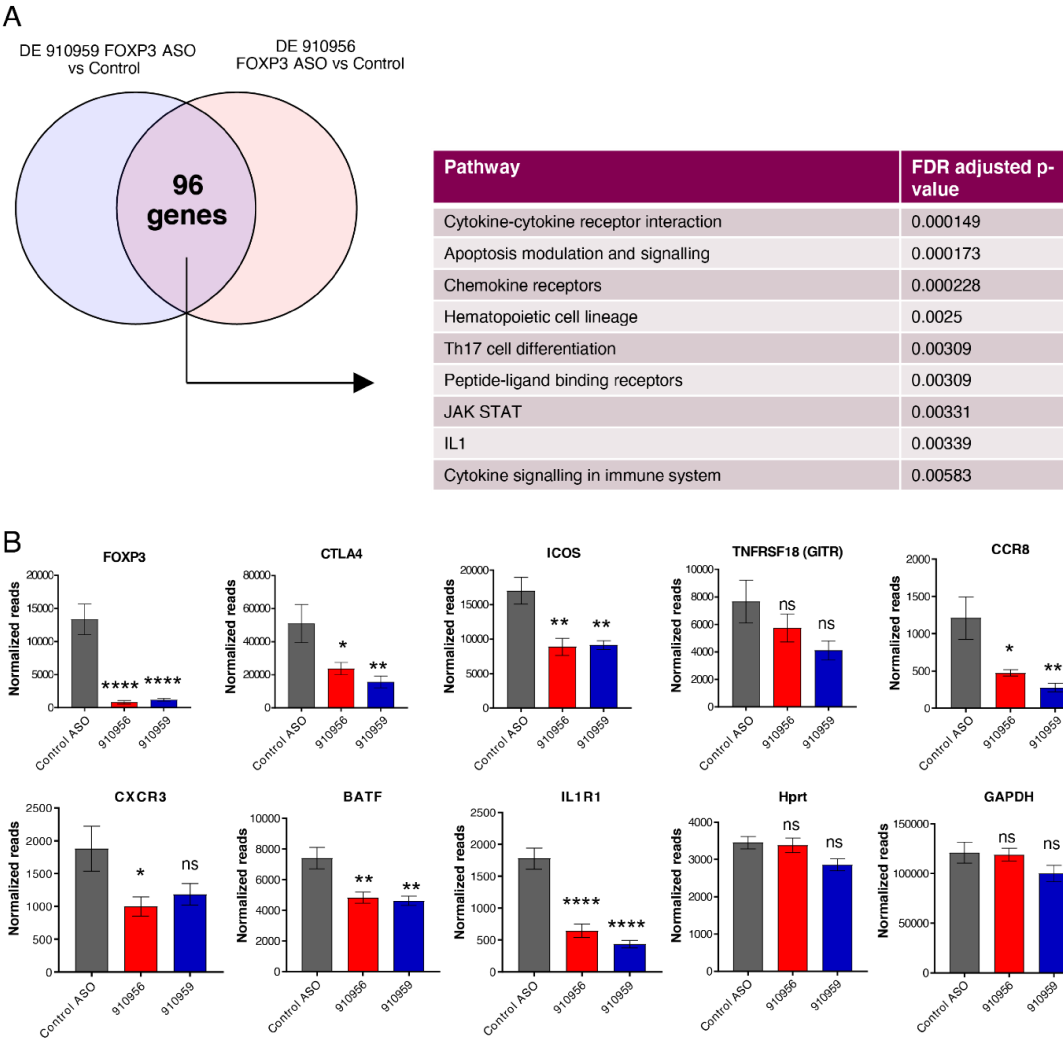
Supplementary Figure 1.



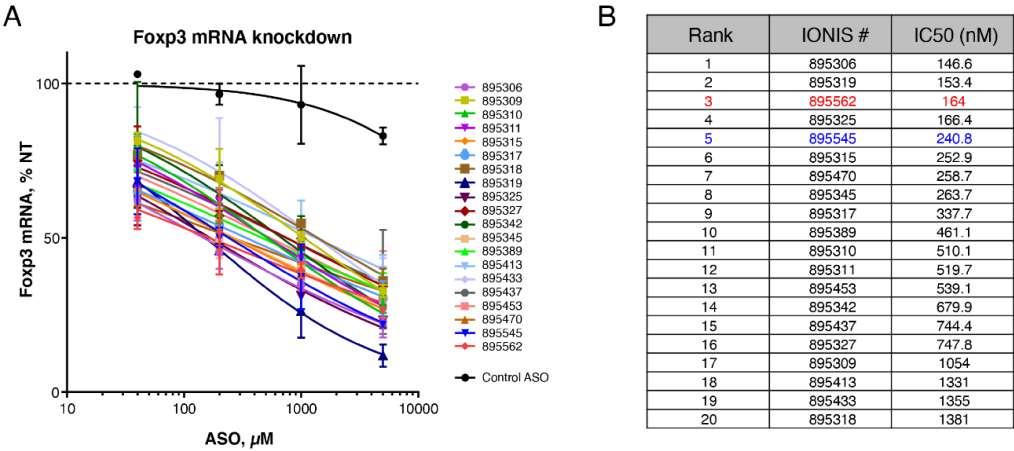
Supplementary Figure 2.



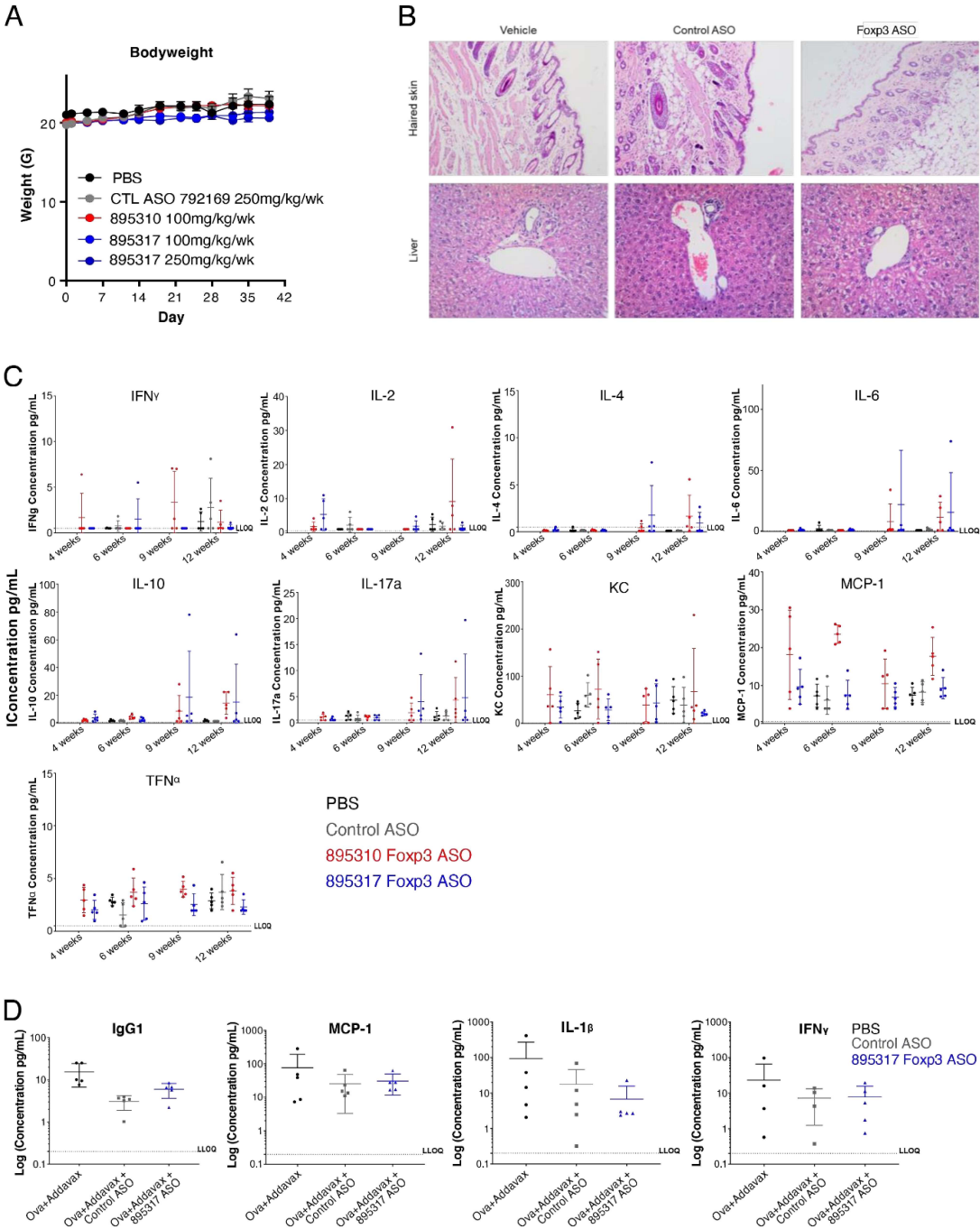
Supplementary Figure 3.



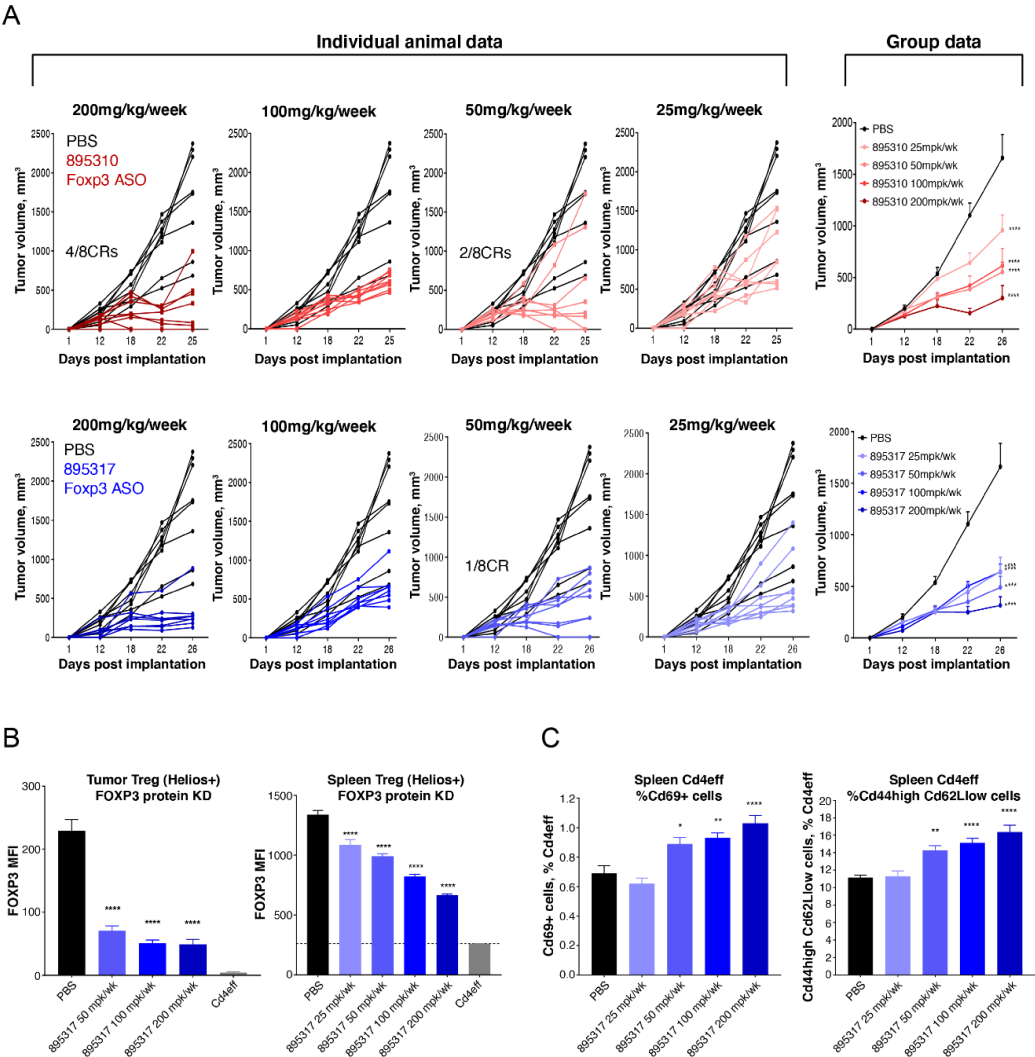
Supplementary Figure 4.



Supplementary Figure 5.



Supplementary Figure 6.



Supplementary Figure 7.

